TOPICAL REVIEW • OPEN ACCESS

Recent progress on the efficiency and stability of lead-free $Cs_2AgBiBr_6$ double halide perovskite solar cells

Physica Scripta

TOPICAL REVIEW

Recent progress on the efficiency and stability of lead-free $Cs_2AgBiBr_6$ double halide perovskite solar cells

Md Jakir Hossen[1,2], **Hairul Mardiah Hamzah**[1], **Md Shahinuzzaman**[3,4], **MS Jamal**[3], **Suhana Mohd Said**[1], **S F W M Hatta**[1,5], **Md Helal Miah**[6], **Mayeen Uddin Khandaker**[7,8] and **Mohammad Aminul Islam**[1,9]

[1] Department of Electrical Engineering, Faculty of Engineering, Universiti Malay, Jalan Universiti, 50603 Kuala Lumpur, Selangor, Malaysia
[2] Department of Physics, Hajee Mohammad Danesh Science and Technology University, Dinajpur 5200, Bangladesh
[3] Institute of Energy Research and Development, Bangladesh Council of Scientific and Industrial Research (BCSIR), Dhaka 1205, Bangladesh
[4] Department of Electrical and Electronic Engineering, Uttara University, Dhaka 1230, Bangladesh
[5] Centre of Printable Electronics, Universiti Malaya, 50603, Kuala Lumpur, Malaysia
[6] Department of Physics, Bangabandhu Sheikh Mujibur Rahman Science and Technology University, Gopalganj-8100, Bangladesh
[7] Centre for Applied Physics and Radiation Technologies, School of Engineering and Technology, Sunway University, 47500 Bandar Sunway, Selangor, Malaysia
[8] Department of General Educational Development, Faculty of Science and Information Technology, Daffodil International University, DIU Rd, Dhaka 1341, Bangladesh
[9] Miyan Research Institute, International University of Business Agriculture and Technology (IUBAT), Dhaka, 1230, Bangladesh

E-mail: aminul.islam@um.edu.my

Keywords: efficiency, stability, lead-free, $Cs_2AgBiBr_6$, fabrication technique

OPEN ACCESS

RECEIVED
18 July 2024

REVISED
26 November 2024

ACCEPTED FOR PUBLICATION
6 December 2024

PUBLISHED
27 December 2024

Abstract

Within a decade, the power congversion efficiency (PCEs) of metal-halide perovskite solar cells (PSCs) moves upward from 3.9% to 25.7%, making them competitive with current state-of-the-art silicon-based counterparts. This steepest growth of the PCEs suggests that the commercialization of this technology might be easing the energy transition from fossil fuel to renewable energy. However, a wide range of factors restrict the commercial viability of PSCs like their toxicity and instability. A crucial and difficult task in the field of PSCs is the replacement of Pb-based perovskite with non-toxic and eco-friendly material while maintaining high-performance with improved stability. $Cs_2AgBiBr_6$ halide double perovskites (HDP) material seems to be very promising in this regard. This article reviews the recent progress in $Cs_2AgBiBr_6$ double PSC devices, especially fabrication techniques including the advancement of its efficiency and stability. Here, the evolution of $Cs_2AgBiBr_6$ towards the application and fabrication of PSCs has also been discussed. This study also analyzed the impact of numerous environmental stresses, such as mechanical, thermal, and optical stresses including the potential prospects in the case of Pb-free PSCs.

Nomenclature

DC	Direct Current
DSC	Differential Scanning Calorimetry
DL	Diffusion Length
ETL	Electron Transport Layer
GTF	Goldschmidt Tolerance Factor
HI	Hot Injection
HTL	Hole Transport Layer
HDP	Halide Double Perovskite
IJP	Inkjet Print
LED	Light Emitting Diode

NC	Nanocrystal
PCE	Photo Conversion Efficiency
PL	Photoluminescence
PSC	Perovskite Solar Cell
RT	Room Temperature
SLME	Spectroscopic Limited Maximum Efficiency
SOEC	Second Order Elastic Constant
SQL	Shockly-Queisser Limit
SPC	Spin Coating
SPCE	Stabilised Power Conversion Efficiency
SVDM	Sequential Vapor Deposition Method
TE	Thermal Evaporation
TGA	Thermogravimetric Analysis
UV	Ultra-Violet
VE	Vacuum Evaporation
XRD	X-ray Diffraction

1. Introduction

Due to low cost, favorable electrical and optical characteristics, and potent light absorption, perovskite solar cells (PSCs) have attracted a great attention from last decade [1]. Moreover, perovskite thin films exhibit tremendous optical and electronic properties, i.e., small trap density, longer diffusion length, low carrier effective mass, high light absorption, tuneable direct bandgap, and easy solution processing fabrication and Pb-based perovskite PSCs have achieved up to 25.7% of PCE within only a few years [2, 3]. Also, all the above mentioned favorable properties make the perovskite a versatile material for several other applications, such as memristors, light emitting diode (LED), photo detectors, photo-catalysis, x-ray detectors, and solar cells. However, despite all the remarkable properties, the perovskite material and solar cells are found to be unstable, and commonly used Pb-based perovskite has a toxic element Pb which obstructed the future commercialization of these materials [4–6]. Particularly, the perovskite layer as well as other supportive layers are influenced by ambient moisture, oxygen, and Ultraviolet (UV) light, and decomposed which leads the device instability. To stabilize the device, several attempts have also been reported, such as modifying device structure; encapsulate the cell, and identifying the optimal Pb-free material. For instance, it has been reported that the replacements of Methylammonium (MA^+) by Cesium (Cs^+) enhanced the decomposition energy by about 0.042 eV, which tremendously increases its stability [7].

Numerous scientists are trying to resolve the toxicity problem in perovskite films by replacing Pb-based materials to other types of materials. It should be noted that primary concept was try to replace Pb with Sn, however, substitution of Pb^+ by Sn^{2+} induces an oxidation problem where Sn^{2+} can easily oxidize and becomes Sn^{4+}. Particularly, a novel and effective technique is to replace lead ion (Pb^{2+}) with B^+ and B^{3+} metal cations, which have the generic chemical formula $A_2B^+B^{3+}X_6$ and are known as double perovskite. Since the unit cell is twice that of lead halide perovskites, halide double perovskites (HDP) got their name. Due to their exceptional stability and optoelectronic qualities, among all the potential and proposed lead-free perovskite structures, HDPs have gained attention and opened up new possibilities for solar cell applications. With the generic chemical formula $A_2BB'X_6$, it has been predicted that more than 100 HDPs could be thermodynamically stable within a tolerable range by combining different A, B^+, B^{3+}, and X components. Where, A = organic or alkali metal ion that is cationic; such as methyl ammonium, Potassium, Rubidium, or Cesium; B^+ = B is an ion of an alkali metal or a transition metal atom in its +1 oxidation state, such as Lithium, Sodium, Potassium, Rubidium, Cesium, Copper, Silver, etc; B^{3+} = In the +3 oxidation state, a transition or main group metal ion; such as Aluminium, Gallium, Bismuth, Indium, etc and X = Halide ions; such as Fluorine, Chlorine, Bromine, Iodine) by several researchers [8]. A-site cations are found in the cavities created by the octahedra in the double perovskites, which have a 3D structure like that of Pb perovskites with alternating $[B^+X_6]^{5-}$ and $[B^{3+}X_6]^{3-}$ octahedra arranged in a 3D framework known as rock salt order (figure 1). Most HDPs crystallize with a cubic crystal structure $Fm\bar{3}m$ with a lattice parameter of 10–12 Å [8–10]. Several HDPs have been studied extensively, such as Cs_2AgBiX_6 [11–13], Cs_2NaSbX_6 [14], and Cs_2AgInX_6 [15]. Among them, $Cs_2AgBiBr_6$ is the leading contender for Pb-free perovskite solar cells due to its numerous encouraging qualities, such as its extended

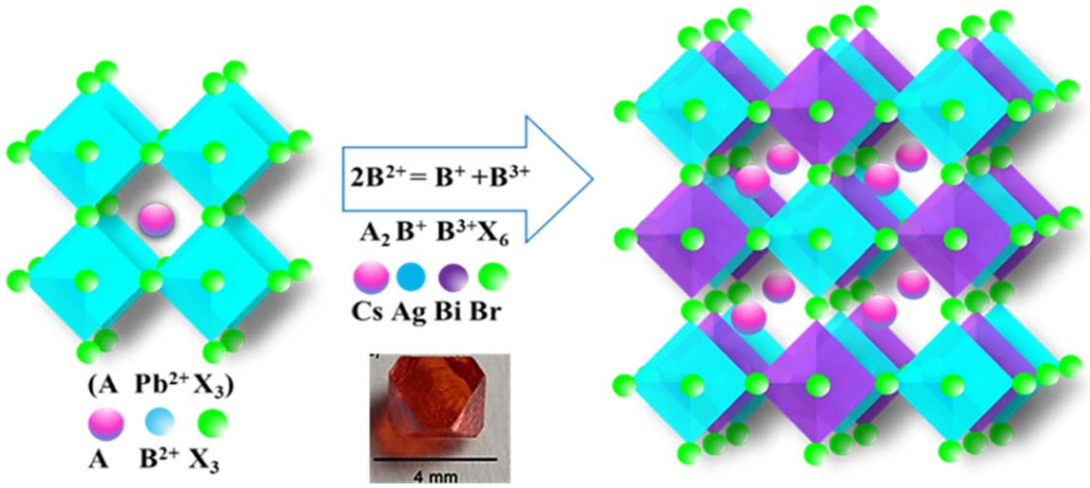

Figure 1. The $Cs_2AgBiBr_6$ crystal structure; the atoms of Bi, Ag, Cs, and Br are represented by different colored spheres, an image of a single crystal of $Cs_2AgBiBr_6$ is shown in inset. (Reproduced with permission from Obada *et al* 2023) [9].

carrier lifetime (660 ns) and resemblance to $MAPbX_3$ [11], high heat and moister stability, a high defect tolerance, low toxicity, an incredibly long radiative emission lifetime of hundreds ns, and low carrier effective mass (0.14 m_e) which is very close to those for $CH_3NH_3PbI_3$ [15].

The first HDP $Cs_2AgBiBr_6$ have been synthesized by Slavney *et al* in 2016, which has a space group of $Fm\bar{3}m$ and bandgap range 1.95–2.19 eV by UV–vis [11, 16–18]. The black $Cs_2AgBiBr_6$ crystals have also been synthesized with a lower bandgap range of 1.69–1.72 eV, which may be arises due to the Ag–Bi disorder [19]. Importantly, very low photoluminescence quantum yield (PLQY) about 0.08% measured for HDP yet which may be due to their indirect bandgap [20]. Beyond PLQY, the diffusion length (DL) and their carrier lifetime are also very important factor for the application in the photovoltaic. Ning *et al* showed that the photoexcitation diffusion length (DL) was about $\approx 110 \pm 20$ nm in the case of $Cs_2AgBiBr_6$ thin films for electrons and holes for the PL quenching model and average photoexcitation mobility was estimated to be $0.37 \pm 0.15\ cm^2V^{-1}s^{-1}$, in the TRPL experiments [21]. The de-trapping of shallow states of the charges or the recombination of $Cs_2AgBiBr_6$ could be responsible for the large photoluminescence (PL) decay time (600 ns) [11, 22]. According to Biega *et al* in 2021, the carrier DL can be up to 1 μm in the case of $Cs_2AgBiBr_6$ crystal which was measured by stroboscopic scattering microscopy method [23]. Because of the lower defect density in a single crystal, this value is significantly larger than that of the thin film. Hoye *et al* in 2018, discovered that the fundamental lifetime of the $Cs_2AgBiBr_6$ thin film is 1.4 μs using transient absorption spectroscopy. According to their findings, $Cs_2AgBiBr_6$ transport characteristics may be able to accommodate thicker active layers, which would result in higher PCEs and current densities due to improved light absorption [24]. Beyond the charge transport and extraction efficiency, $Cs_2AgBiBr_6$ thin films are also processes relatively very low carrier effective masses which crucially need to be improved for high efficiency PSCs [25].

It should be emphasized that not every candidate of HDP has a stable structure. A perovskite structure can be formed depending on (1) the octahedral factor (μ) and (2) the tolerance factor (t) [26]. Goldschmidt Tolerance Factor (GTF) is generally adopted for the calculation of the crystallographic stability of the HDP structure by t [27] and μ [28] To become a stable structure of a HDP, the GTF and Octahedral factor μ must be within $0.81 < t < 1.11$, and $0.41 < \mu < 0.90$, respectively [27]. In the case of $Cs_2AgBiBr_6$ HDP, GTF is $t = 0.890$, and the octahedral factor for the octahedron $[AgBr_6]^{5-}$ is $\mu = 0.587$ [28]. On the other hand, if the decomposition energy (ΔH) is positive, then the material is more stable rather than a negative one. Interestingly, CsBr, AgBr, Cs_2AgBr_3, $CsAgBr_2$, and $Cs_3Bi_2Br_9$ have estimated positive decomposition energies, which are higher than $MAPbI_3$ and indicate a higher thermodynamic stability. Particularly, in $Cs_2AgBiBr_6$, Pb^+ cations have been replaced by Ag^+ and Bi^{3+} cations, as they have enhanced Coulomb interaction energy which induces more positive decomposition energy (+0.38 eV) [29]. Subsequent investigation demonstrated that Cs_2AgBiI_6 was not stable because of negative value of $\Delta H = -0.41$ eV was observed. Figure 1 shows the crystal structure of $Cs_2AgBiBr_6$ including a photograph and edge sharing tetrahedral structure mode.

In $Cs_2AgBiBr_6$, there are four distinct lattice sites, and the ionic substitution offers a wide range of opportunities to carefully control their photovoltaic properties. For instance, adding the S element to the film can significantly improve its ability to capture light and its photovoltaic performance [30]. A spin-coated $Cs_2AgBiBr_6$ film-based perovskite solar cells were reported in 2017 and experimentally proved the feasibility of halide double perovskites for solar cells (PCE = 2.43%) [12]. According to the Shockley-Queisser limit (SQL),

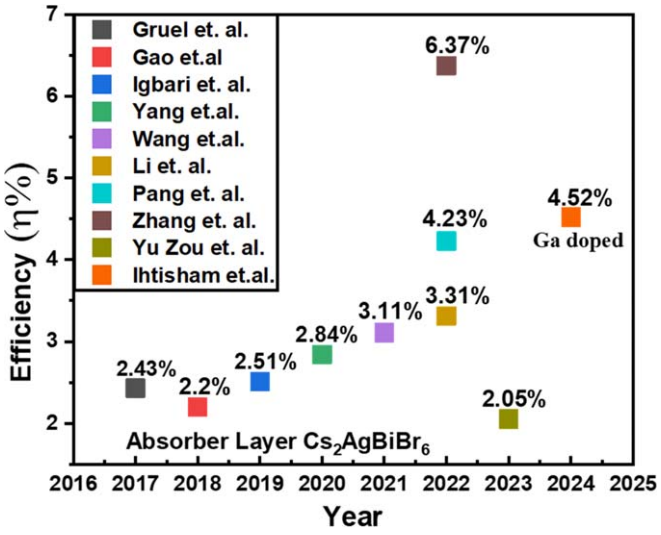

Figure 2. Efficiency of $Cs_2AgBiBr_6$-based solar cell.

the maximum efficiency could be 7.92% for $Cs_2AgBiBr_6$ (200 nm) solar cells due to their relatively large and indirect bandgap [29]. According to Islam *et al* by tuning the valence band between the $Cs_2AgBiBr_6$ absorber (600 nm) and Cu_2O HTL, a higher simulated PCE of 11.17% can be achieved [31]. The efficiency could be improved further via doping with appropriate materials, which has been discussed later. For instance, low PCEs resulting from poor visible light absorption, subpar film quality, substantial defects, and wide indirect bandgap are a remaining issue for solar cell applications. Front the current art of work, the PCE of $Cs_2AgBiBr_6$ film is often lower than 4.23% due to the broad bandgap of the material [32]. Zeyu Zhang and his co-researchers achieved a state-of-the-art champion efficiency of 6.37% so far by employing a post-treatment hydrogenation method of $Cs_2AgBiBr_6$ films with the tunable bandgap from 2.18 eV to 1.64 eV, with long environmental stability. Figure 2 shows the experimentally fabricated solar cell PCE from 2017 to 2024, where the highest PCE of 6.37% was reported by Zhang *et al* in 2022 [32]. Most recently Ihtisham et al in 2024, were able to lower the band gap from 1.91 eV to 1.86 eV by Ga doping perovskite layer [33]. As a result, the overall efficiency increased from 3.51% to 4.52%, which shows significant improvement over the pure solar cell. Asad et al in 2024, were able to lower the E_g from 1.91 eV to 1.82 eV by Al doping with perovskite layer $Cs_2AgBiBr_6$. The current-voltage (J-V) curve indicates that the undoped solar cell had an efficiency of 3.02%, a Voc of 0.89 V, FF of 0.67, and Jsc of 5.01 mA cm^{-2}. Improvements were seen when Al was doped; Voc increased to 0.91 V, FF to 0.71, and Jsc to 5.29 mA cm^{-2} and the output efficiency increased to 3.40% [34].

Particularly, enormous efforts have been made to optimize and enhance the optoelectric properties of the $Cs_2AgBiBr_6$ absorber layer, however, the PCE of the complete solar cell is yet to be below 7%. To mitigate the limitations and improve solar cell efficiency, the inherent limits of this material must be examined through several investigations and analysis. Consequently, a thorough review is required to determine the properties of this novel absorber material, the experimental obstacles, and its promises. Previously, several review works have been done related to this field where the fragmented information was gathered. Table 1 presents the list of related review works. Most of the review covers the optoelectronic properties and their physical structure, bandgap engineering, interface, and additive engineering of $Cs_2AgBiBr_6$ HDPs. However, there were very few discussions on synthesis and fabrication issues, especially its stability. In this study, the effect of the synthesis or fabrication process of $Cs_2AgBiBr_6$ on the solar cell performances was discussed largely and then the various stability issues were analyzed and discussed up to date elaborately than any other available reported literature listed in table 1. Finally, the future perspectives and major challenges faced by $Cs_2AgBiBr_6$ materials have been discussed focusing on the feasible solutions that could lead to the improvement of nontoxic, highly stable, and low-cost PSC.

2. Fabrication techniques of $Cs_2AgBiBr_6$-based PSCs

In general, the fabrication processes of $Cs_2AgBiBr_6$ materials are quite simple rather to any other perovskite material. Several fabrication techniques, including vacuum evaporation [41], hot injection [32, 40, 42], inkjet-printing [43], spin-coating [32], and spray coating [44], etc have been developed so far to address the limitations of making lead-free HDP materials. It has been revealed through research conducted in the recent few years that

Table 1. List of related published review articles.

No.	Title	Journal	Scope & limitations	Year	References
1	Fundamental understanding of the performance-limiting factors of $Cs_2AgBiBr_6$-based perovskite photovoltaics	Renewable and Sustainable Energy Reviews	Absorption Capability, Bandgap regulation, Film morphology, Interface control, Additive engineering. No discussion on the Synthesis process, Stability	2024	[35]
2	Advancing Lead-Free $Cs_2AgBiBr_6$ perovskite solar cells: Challenges and strategies	Solar Energy	Very short discussion on the fabrication process and bandgap modulation	2023	[36]
3	$Cs_2AgBiBr_6$ Double Perovskites as Lead-Free Alternatives for Perovskite Solar Cells.	Solar RRL	Discussion on the limitations of HDP solar cells, and charge transport and recombination	2022	[37]
4	Properties, performance, and multidimensional applications of stable lead-free $Cs_2AgBiBr_6$ double perovskite	Materials Today Physics	Opportunities and obstacles of diff. application. Structural behavior charge carrier dynamics, transport layers, Brief discussion on the fabrication process	2022	[38]
5	Recent progress of lead-free halide double perovskites for green energy and other applications	Applied Physics A	Evaluations of the optical, electrical, magnetic, thermoelectric, structural, mechanical, and thermal stabilities of lead-free HDP and its applications, both theoretical and experimental.	2022	[39]
6	Lead-free double perovskite $Cs_2AgBiBr_6$: fundamentals, applications, and perspectives	Advanced Functional Materials	Structure-property relation, stability, bandgap modulation, and application highlighted	2021	[25]
7	Recent advances in $Cs_2AgBiBr_6$-based halide double perovskites as lead-free and inorganic light absorbers for perovskite solar cells	Energy & Fuels	Enhancing optoelectronic properties through bandgap and interface engineering; a brief description of the synthesis and fabrication process; structural, photoelectric, and physical attributes.	2020	[40]

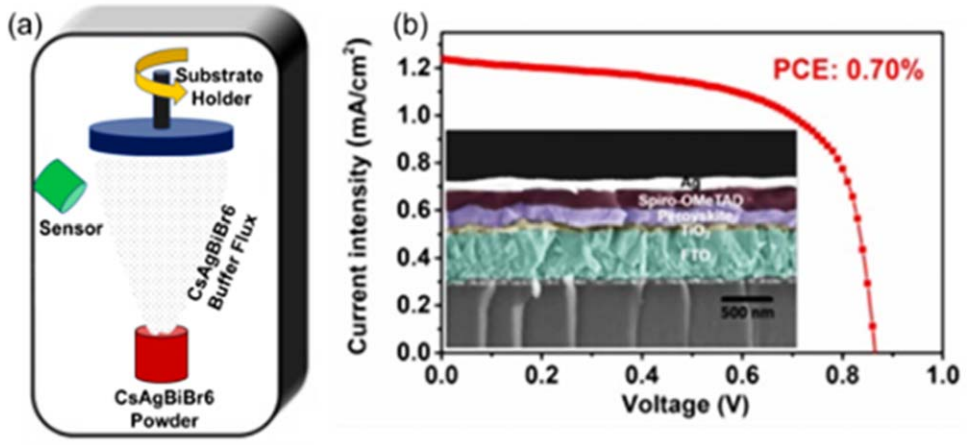

Figure 3. (a) Schematic image of vacuum evaporation technique for film fabrication, and (b) PSC structure and J-V characteristics of single-source vapor-deposited $Cs_2AgBiBr_6$ thin films for Lead-Free PSC reported in Fan *et al* 2016 . Reproduced from [48]. CC BY 4.0.

a variety of deposition and synthesis methods can be used to control crystallinity, thin film orientation, and optoelectronic behavior in both single crystals and thin films which can improve cell performances [37]. Also, the optoelectronic properties like chemical bond, energy level, crystallinity, mobility, conductivity, atomic arrangement, and so forth solely depend on the specific synthesis method [25]. $Cs_2AgBiBr_6$ perovskite material was first synthesized by Slavney *et al* in 2016 with an indirect bandgap of 1.95 eV and a long carrier lifetime of 660 ns [11]. Then Gruel *et al* in 2017 fabricated experimentally the first solar cell with PCE 2.43% [12]. Although the stoichiometric ratios of the elements were proposed to influence the performance of solar cells, theoretical predictions regarding its impact on the optoelectronic properties do not provide a consistent picture [45, 46]. Here we are going to discuss different fabrication methods and their pros and cons in brief.

2.1. Vacuum evaporation

Vacuum evaporation (VE) is a popular technique for fabricating a thin film. In the VE technique, the solid source material is heated at a high temperature to evaporate in a vacuum allowing vapor particles directly reach to substrate, where they solidify again [47]. This technique used a solid or powdered material-holding boat or resistive coil. To reach the high melting temperatures necessary for metal evaporation, a high direct current (DC) is applied to the resistive boat/coil. The material's evaporation and transportation to the substrate are facilitated by the high vacuum (less than 10^{-4} Pa). Particularly, the process is very useful for materials with low melting points. Figure 3(a) shows a schematic diagram of a thermal evaporation system. Thermal evaporation has several benefits, including the ability to produce perovskite thin films without the use of solvents, the capacity to deposit over large areas, can improve and control the material incorporation with repeatable film characteristics, can fabricate thin films with highly crystalline, excellent composition with retained stoichiometry, full surface coverage, and well-defined grain structure [48].

The first pure-phase, high-quality $Cs_2AgBiBr_6$ thin-films were created in 2018 by Wang *et al* using a sequential vapor deposition technique [49]. They deposited AgBr, $BiBr_3$, and CsBr sequentially layer by layer on top of the substrate, and later thermally annealed this multilayer stacks to form the $Cs_2AgBiBr_6$ phase via diffusion reaction. They attained a PCE of 1.37%. Fan *et al* used a vapor deposition process to construct high, ultra-smooth $Cs_2AgBiBr_6$ thin film and attained a photo-conversion efficiency of 0.7% in an ambient environment [48]. They proposed that by maximizing the band to band alignment at the interface between the charge-transporting materials and perovskite, could minimize the carrier recombination loss and the efficiency could be further increased. Moreover, direct bandgap $Cs_2AgBiBr_6$ HDP thin films can fabricate via proper doping that will certainly boost the efficiency of PSCs. It should also be noted that the main limitation of the vacuum evaporation technique is additional point defects arise during $Cs_2AgBiBr_6$ thin film synthesis. It was proposed to fabricate $Cs_2AgBiBr_6$ films directly using multi-source co-evaporation in which the sample is annealed directly at 230 °C. Due to the high annealing temperature and extremely low solubility of organic solvents, the quality of obtained films using this technique is not good enough yet to apply for high efficiency PSCs. Therefore, it is imperative to investigate for the appropriate solvent, and also, the annealing temperature must be optimized to improve the film quality. Additionally, the cooling rate also influenc the film quality and need to be optimized as well [38].

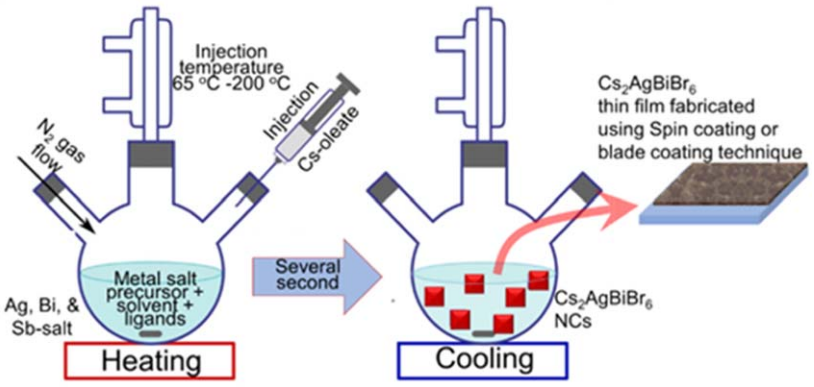

Figure 4. Schematic descriptions of the hot injection methods to synthesize colloidal Cs_2AgBiX_6 NCs and thin film.

On the other hand, the limitation with vacuum deposition is loss of materials that remain inside of the vacuum chamber, and in case of co-evaporation, the rate of deposition for each chemical is different. In conclusion, the results found from the initial vapor deposition to fabricate $Cs_2AgBiBr_6$ thin films seem promising, additional investigation is necessary to improve the generation of pure Cs2AgBiBr6 HDP film. This includes investigating the co-evaporation and optimize for each materials, condition of substrate heating during vapor deposition, and post-annealing conditions. Proper control of the deposition parameters is required by changing and/or lowering the deposition rate, ambient pressure, and annealing temperature for the HDP thin films which can control and/or reduced to generate some of the side phases (such as AgBr, $Cs_3Bi_2Br_9$) [49]. These phases influence the films' properties as well as thermodynamic stability.

2.2. Hot injection

The Hot injection (HI) method provides an easy synthesis protocol to convert cubic NCs to hexagonal NCs and these NCs are used to fabricate thin film using other techniques like spin coating or blade technique. Particularly, highly crystalline $Cs_2AgBiBr_6$, $Cs_2AgBi_{0.6}Sb_{0.4}Br_6$ nanocrystals, and quantum dots can be obtained using fabrication processes like hot-injection, and ligand-assisted re-precipitation method [32, 40, 42]. The brief description of the $Cs_2AgBiBr_6$ film fabrication is schematically shown in figure 4. Kumar *et al* reported that the size of the NCs of $Cs_2AgBi_{0.6}Sb_{0.4}Br_6$ decreased as $Cs_2AgBiBr_6$ is doped with Sb [42]. The reducing the NC size is related to the different ionic radius and the molar ratio of Bi^{3+} and Sb^{3+} (ionic radius 117 pm and 90 pm; molar ratios 0.45 and 0.4, respectively). The change in the bromide precursor's injection temperature during colloidal synthesis may also be responsible for the reduction of size. Apparently, there have been reports that the spin-coated thin film using $Cs_2AgBi_{0.6}Sb_{0.4}Br_6$ NCs exhibit smooth, compact, and without pinholes topography, however, the reported PSC of the p-i-n structure showed very low PCE (0.09%) [42]. Furthermore, the PCE of PSC could be improved via effective surface state passivation to reduce trap-assisted recombination and band-to-band matching between the charge transport layers.

2.3. Inkjet printing

Over the past few years, PCEs in PSCs with an Inkjet print (IJP) perovskite absorber layer have been continuously rising. The PCEs of Pb-based PSCs have reached over 21% in single scan tests and over 18% in stabilized power conversion efficiency (SPCE) [50, 51]. It should be noted that the PCE of PSCs also depends on the fabrication technique of supportive layers, such as electrodes, ETLs, and HTLs. Unlike many other deposition methods for translating to industrial-scale manufacturing, the IJP deposition allows to fabrication of all stack layers as well as allows maintenance or even expansion of design advantages. For each layer, the ink characteristics, inkjet settings, and annealing process are needed to be optimized. It has been reported that the PCE of PSCs with inkjet-printed absorbers and charge carrier extraction layers was found to be over 17% with little hysteresis [50]. The devices printed in an ambient environment that exhibited exceptional short-term stability (40 h) were tested using a high temperature of 85 °C. These findings represent an encouraging next step towards fully inkjet-printed PSCs with large commercial sizes. Figure 5 presents the schematic image of the Inkjet printing technique for film fabrication.

Even though IJP electron transport layers (ETLs) [52] and hole transport layers (HTLs) [53–55], have been reported, however, fully developing IJP PSCs is still difficult due to the wide range of complexities that arise concerning solvent-material interactions, formation of thick films, wetting behavior, as well as limits in the annealing temperatures of each layer when processed on top of the underlying layers. These solvent-rich layers

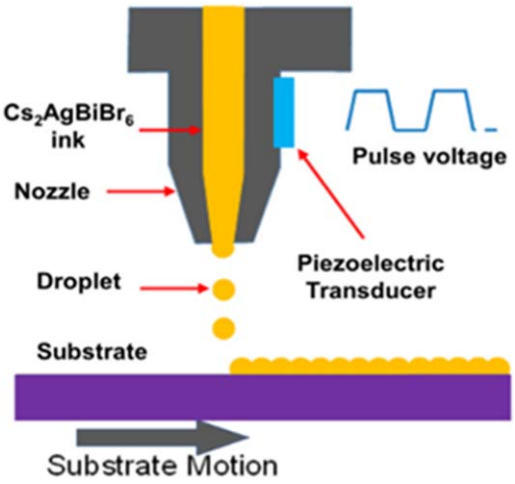

Figure 5. Schematic image of Ink Jet printing technique for film fabrication.

are unsuitable for producing compact, crystalline films that are homogeneous in thickness. Zhang *et al* fabricated a picoliter-sized droplet inkjet printing technology to resolved the issues with the pricey vacuum-assisted annealing stage [55]. The combined Lead acetate ($PbAc_2$) and lead chloride (MACl) have been reported to fabricate the perovskite thin films using IJP technique. However, $PbAc_2$ is changed during the reaction process to methylammonium acetate (MAAc), which is supposed to be more flammable than methylammonium chloride (MACl). The preferred crystal structure was determined by the equilibrium between the quantities of $PbAc_2$ and $PbCl_2$. Using IJP perovskite film with a thickness of 1.6 μm, the reported PCE of PSC was 16.6% [56].

2.4. Spin coating

Spin coating technique is a great way to fabricate a thin and homogeneous thin film on a flat substrate. At the center of the substrate, which is spinning slowly or not at all, a tiny amount of liquid coating material is usually applied. The substrate is then rotated in a suitable rpm and liquid is spread over the substrate surface due to the centrifugal force and coat a thin film. In the case of perovskite material, fabrication must be needed to use in a glove box to avoid the impact of moisture and oxygen [57].

Even most research work relevant to PSCs were reported using spin coating techniques, however, there are numerous benefits as well as drawbacks belongs to this method. Wang *et al* in 2016 demonstrated that one-step spin coating in ambient air can't be commonly employed for high-efficiency PSCs [57]. It has been reported that the solution processing of $Cs_2AgBiBr_6$ absorber materials in open air will be induced vacancies, interstitials, and/or antisites defects with lattice disorder. On the other hand, spin-coating results in a significant waste of materials, increasing the cost. According to Daem et al in 2021, it is possible to prepare or deposit high-quality $Cs_2AgBiBr_6$ films by careful controls of the precursor stoichiometry using one-step spin-casting fabrication methods. Alternatively, Igbari *et al* in 2019 demonstrated that the solution processes synthesis method is superior to the vacuum sublimated technique [44]. By spin-coating, on top of the mesoporous (mp)TiO_2/polymethylmethacrylate-coated substrates, McClure *et al* (2016) created a $Cs_2AgBiBr_6$ powder-based device with a PCE of 0.77%. Using in situ spectroscopy and diffraction, the growth of the $Cs_2AgBiBr_6$ layer was investigated during spin coating and the subsequent post-deposition thermal annealing. It has been observed that dropping of antisolvents during the substrate spinning causes the wet film to instantly become supersaturated and crystallize. However, it is important to know that the timing of the antisolvent drop influences formation dynamics of the films and it's final microstructure [16, 57]. Figure 6(a) shows the schematic diagram of the solution-processed antisolvent dropping spin coating method with post-plasma treatment. Figure 6(b) shows the schematic diagram with the IPA drop-coated $Cs_2AgBiBr_6$ film fabrication process [57]. The solution-processed $Cs_2AgBiBr_6$ thin film exhibited has a maximum photo-conversion efficiency of 2.51% [44].

At first Z. Zhang *et al* in 2022 fabricated (figure 8(a)) high-quality and smooth surface $Cs_2AgBiBr_6$ thin films using a conventional one-step spin-coating solution process and by using a post-crystallisation hydrogenated process. Their champion cell showed PCE of about 6.37% [32]. Plasma treatment with various times (600 s and 1200 s) was introduced to dope by the hydrogen atoms to the fabricated high quality perovskite films [32]. The color of the film has changed from yellow to black (insert photos in figure 7(a)) with the increase of time, indicating the increase in light absorption by the film significantly. Also, perovskite film with a smooth surface

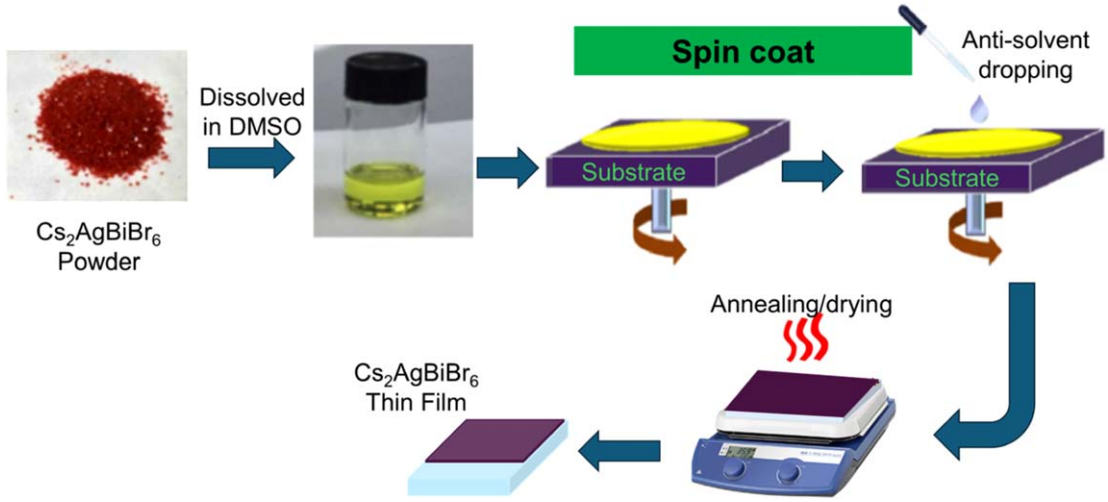

Figure 6. Schematic diagrams of the spin coating fabrication techniques of $Cs_2AgBiBr_6$ thin films.

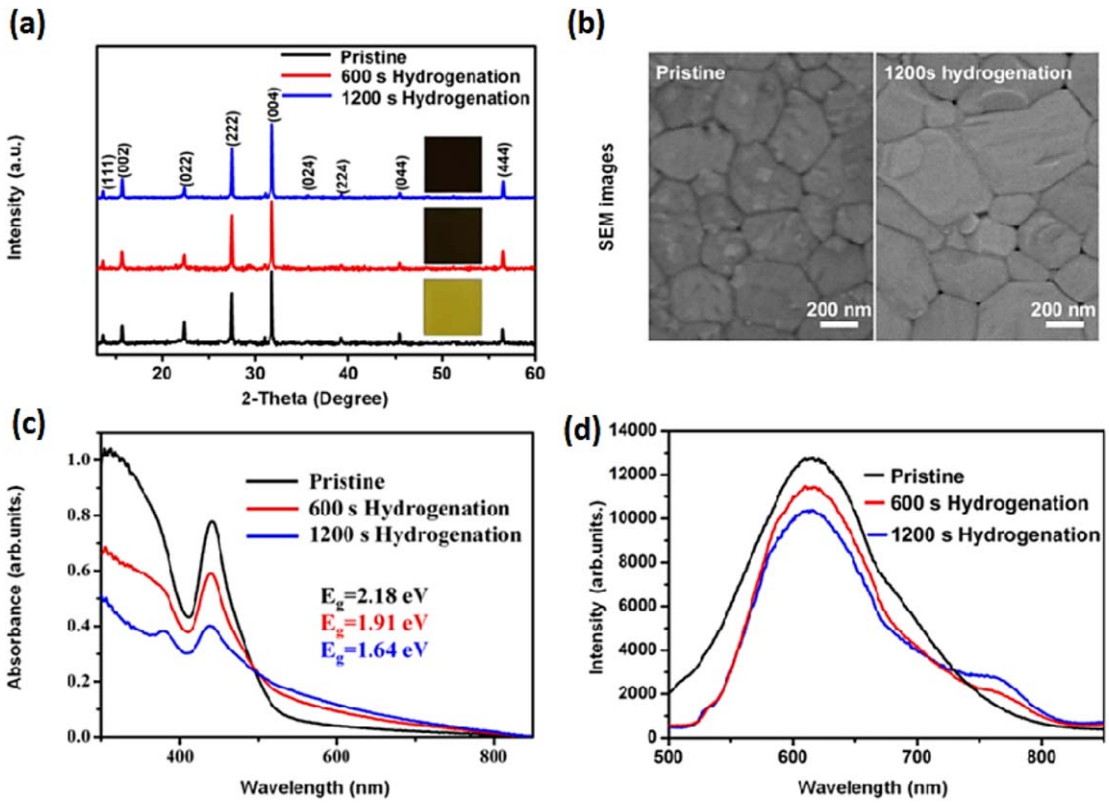

Figure 7. (a). XRD patterns of the $Cs_2AgBiBr_6$ perovskite films and their optical visualization with different hydrogenation times. (b). $Cs_2AgBiBr_6$ film morphology with and without hydrogenation by SEM images. (c) UV-Vis absorbance peak with the corresponding bandgap of $Cs_2AgBiBr_6$ perovskite films. And (d) PL spectroscopy of $Cs_2AgBiBr_6$ perovskite films (Reproduced with permission from Z. Zhang *et al* 2022). Reproduced from [32]. CC BY 4.0.

and bigger grains has been achieved via hydrogenation for 1200 s (figure 7(b)), without any phase transition as shown in figure 7(c). Although their bandgap values have fallen from 2.18 eV to 1.64 eV, the treated $Cs_2AgBiBr_6$ films are still indirect semiconductors after being hydrogenated for 600 and 1200 s. After hydrogenation, the $Cs_2AgBiBr_6$ films were aged in a variety of conditions, such as 20 °C/N_2/dark, 20 °C/N_2/1-sunlight-illumination, and 85 °C/N_2/dark. After that, optical images of the hydrogenated $Cs_2AgBiBr_6$ films were taken at various times to determine their bandgap values using UV-Vis. Additional research verified that atomic hydrogen interstitial doping in the $Cs_2AgBiBr_6$ lattice might optimize carrier mobility and lifespan in addition to adjusting its valence and conduction band energy levels [32].

2.5. Spray coating

Besides the stability issues, another biggest challenges for the commercialization of the PSCs are their limitation of large-scale fabrication suitability. Also, to minimize the cost of production of solar cells, large-area fabrication is crucially needed. Since most of the reported fabrication processes including spin coating are ineffective with roll-to-roll manufacturing processes and difficult to duplicate, and it is well acknowledged that large-scale PSC development is not possible. To resolve these issues, the Spray coating method is usually used **t**o create a large-area perovskite solar cell. In addition, the spray-coating technique can be used to efficiently produce electrodes, HTLs, and ETLs. Usually, there are two types of spray coating steps: (i) Single layer spraying / One step spray-coating, and (ii) Two-step spray coating.

Barrows *et al* were able to achieve higher film surface coverage of 85% and a resulting PCE of 11% for one-step spray-coated devices in 2014. They adjusted the process parameters (such as substrate preheating temperature, and post-annealing temperatures) to increase the effectiveness of single-pass ultrasonic spray coating (USC) carried out in ambient conditions [58]. To develop a single-step procedure with 11.3% PCE, Chang *et al* also investigated the kinetics of the ink production and drying process [59]. Other materials, such as mixed HDP systems or Cs and FA containing mixed cation, can also be coated using the spray coating technique. 17.8% of PCE was confirmed by Bishop *et al* where they fabricated triple-cation (including Cs) PSCs utilizing USC technique. For a while, a low vacuum was applied to partially wet spray-cast films to stop the crystallization of the film. Due to the films being subjected to vacuum-assisted thermal annealing, the process resulted in smooth films containing tiny, densely packed perovskite crystals [60]. Spray-antisolvent (SAS) technique was used in an innovative fabrication based on one-step spray-coating, which took inspiration from the application of anti-solvent, as demonstrated by Yun *et al* Using a metal mesh electrode, a large-scale (16 cm^2) PSC devices was demonstrated with a PCE of 12.1% [61]. It should be noted that the larger active area of PSC devices means larger functional layer and large number of defects. Thus, rate of the extraction of photo-induced carriers are reduced when PSC fabricated in large area and impacted the device performance. Heo *et al* in 2021, recently unveiled a novel spray-coating method that is scalable and orthogonally processable, enabling the fabrication of inorganic $CsPbI_2Br$-based perovskite thin film that exhibited exceptional stability and performance. Due to the graded structure with an aperture area of 112 cm^2, the device with structure (FTO/c-TiO2/CsPbI3-xBrx/PTAA/Au) showed 16.81% of PCE [62].

The deposition of $Cs_2AgBiBr_6$ HDP thin films using spray processing was first reported by N Daem *et al* In their study, the spin-coated benchmark was used to compare the microstructural and optoelectronic characteristics of the spray-coated film. It has been found that ultrasonic spray coating allows to deposit exceptionally smooth and homogeneous thin films with smaller and better-connected grains compared to the spin-coated benchmark. Figure 8(a) shows a schematic diagram of the spray coating method. Figure 8(b) shows the efficiency of both spray and spin-coated film while 8(c-d) represents the morphology of $Cs_2AgBiBr_6$ film. 8(e) represents the cross-sectional view of different layers (Glass/FTO/c-TiO_2 and m-TiO_2/$Cs_2AgBiBr_6$). When $Cs_2AgBiBr_6$ HDP thin films are sprayed-coated, they are reported to have 2.3% of PCE with a high open-circuit voltage (Voc) of 1.09 V, where, Voc of 0.82 V found for spin-coated solar cells [44]. The ultrasonic spray deposition showed strong possibilities to deposit optimum $Cs_2AgBiBr_6$ with high light absorption and charge transfer capabilities; however, more efforts are crucially needed to ensure better infiltration of the spray coating technique.

Two-step spray processing is used in place of dripping processing to facilitate the reaction between MAI and PbI_2. It is significant to remember that the spray deposition of the MAI solution determines the final film morphology. Huang *et al* used a two-step perovskite film deposition process and the coated layers are then heated with a certain temperature. During the thermal heating, the precursor layers are diffused and forming thin films of $MAPbI_3$ perovskite. This process also yields an effective mesoscopic solar cell with 16.0% PCE for an active area of 0.1 cm^2 and 13.1% PCE for 1 cm^2 [63]. Different parameters of the two-step USC method used for perovskite layer deposition were examined by Lan *et al* [64] They investigated the effects of altering variables such as solvent quality, spray precursor solution concentration (PbI_2 and MAI), and post-annealing conditions (temperatures and duration) using a wet chemical process technique [65]. We think that similar two-step process could be feasible for high efficiency Cs-based HDP PSCs.

Furthermore, the benefits of the spray coating techniques such as its adaptability, ease of use, affordability, and strong compatibility utilizing a variety of materials—make it the method of choice for producing PSCs for commercial use. The process has a lot of promise for the large-scale implementation of perovskite devices in the future; however, deeper mechanisms, like those involving the substrates and perovskite precursor solution's properties, coating speed, and annealing procedures need to be investigated and optimized. Particularly, we are far from achieving the expected performance and further research on fabrication techniques is crucially needed to achieve affordable PSCs. Table 2 represents the PSC structure with efficiencies using different fabrication methods.

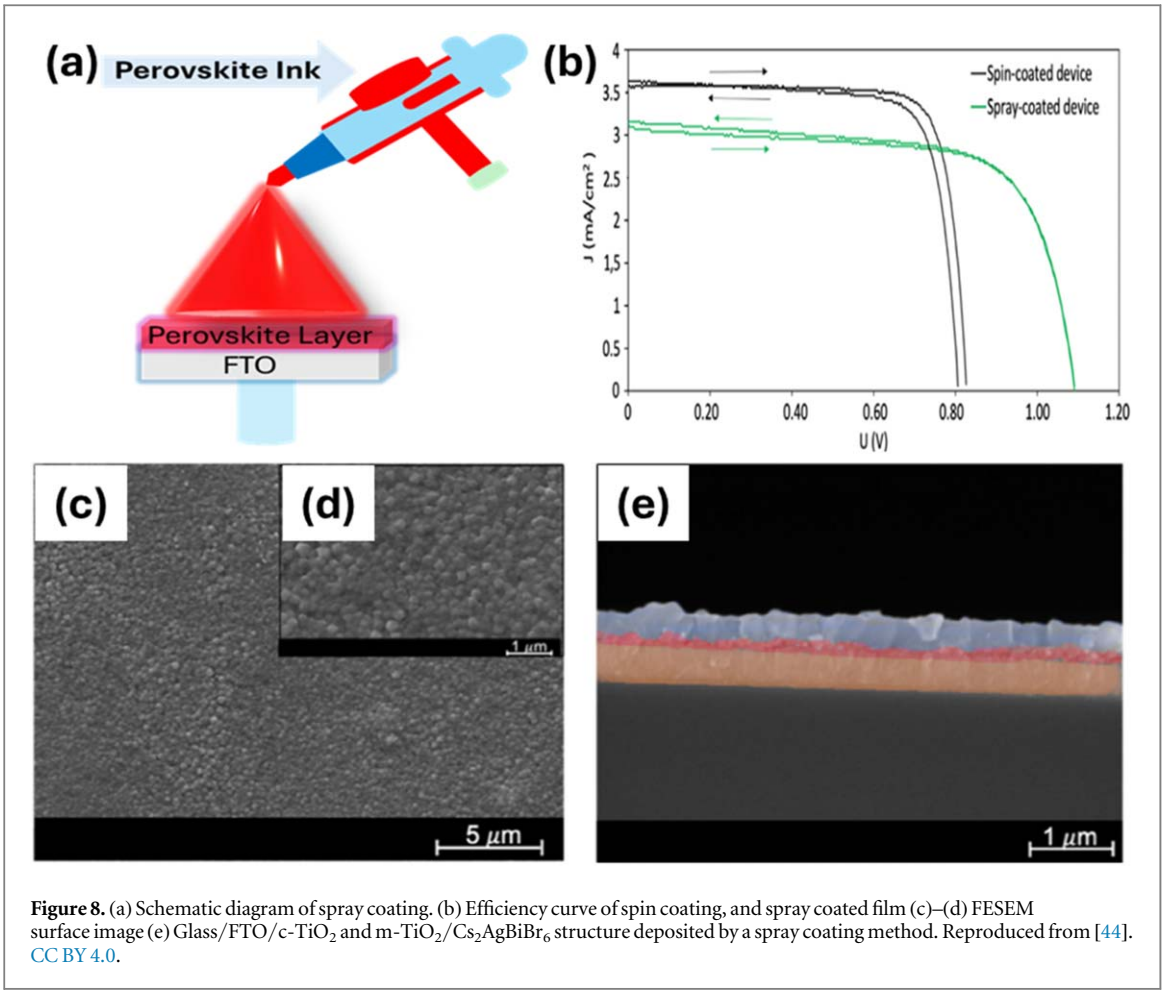

Figure 8. (a) Schematic diagram of spray coating. (b) Efficiency curve of spin coating, and spray coated film (c)–(d) FESEM surface image (e) Glass/FTO/c-TiO_2 and m-TiO_2/$Cs_2AgBiBr_6$ structure deposited by a spray coating method. Reproduced from [44]. CC BY 4.0.

In conclusion, the optoelectronic characteristics of $Cs_2AgBiBr_6$ (such as stoichiometry, energy level, atomic arrangement, conductivity, carrier mobility, etc) are entirely dependent on the particular synthesis method [25]. So far, the most successful method for creating lead-free inorganic perovskite solar cells with higher efficiency is the post-crystallization spin coating hydrogenation procedure, which is the focus of all these investigations. However, spin coating, which involves quickly dropping the HDP solution (often with concentrations of 0.5–0.6 M) on a fast-spinning substrate, has become the most widely employed approach recently [32]. Thus, we anticipate that choosing lead-free HDPs and using the right synthesis technique will result in a higher PCE (%) in the near future [39].

3. Stability

The stability of PSCs refers to their ability to maintain performance and structural integrity over time when exposed to various environmental and operational conditions. While perovskite solar cells have shown great promise in terms of efficiency and cost-effectiveness, they have historically faced challenges related to their stability. Stability is a crucial aspect of perovskite solar cell development because long-term performance and reliability are essential for the commercial viability of this technology. A tremendous amount of work has been done to improve long-term stability, including ion migration, passivating interfaces, adjusting compositions, and creating low-dimensional perovskites [86–88]. Below, we have discussed the factors that can affect the stability of PSCs including chemical, thermal, light- moisture, and mechanical stability of double perovskite.

3.1. Chemical stability

When a substance is subjected to different environmental conditions over time, its ability to retain its chemical composition and qualities is referred to as chemical stability. The conditions that can affect chemical stability include Oxygen and air, pH, chemical compatibility, and time. Oxygen can cause oxidation reactions in many materials, leading to chemical degradation. Changes in pH can influence the stability of substances, particularly those that are acidic or basic. Especially, pH-sensitive materials may degrade under conditions that alter their acidity or alkalinity. The presence of other chemicals, either as contaminants or as part of a mixture, can affect

Table 2. Fabrication methods and their corresponding structure and efficiencies.

Synthesis method	Device structure	*Jsc* (mA/cm^2)	V_{OC} (V)	*FF* (%)	η (%)	References
Solvent Evaporation and Hydrothermal techniques	FTO/BL TiO_2/*mp*-TiO_2 layer/$Cs_2AgBiBr_6$/ Spiro-OMeTAD/Au	1.16	43.9	0.94	2.83	[66]
One step coating	FTO/TiO_2/C_{60}/$Cs_2AgBiBr_6$/PCDTFBT/Au	2.25	1.01	69.3	1.57	[67]
Two-step heating process followed by step coating	FTO/PEDOT: PSS/$Cs_2AgBiBr_6$/N719/SpiroOMeTAD/Ag	5.13	1.06	—	2.84	[68]
One-step solution deposition	ITO/TiO_2/$Cs_2AgBiBr_6$ (205 nm)/Spiro-OMeTAD/ Au	1.7	1.06	74	1.22	[25]
One-step spin coating	TiO_2/$Cs_2AgBiBr_6$/spiro-MeOTAD/ Au	1.7	1.06	74	1.22	[64]
Low-pressure assisted method	ITO/SnO_2/$Cs_2AgBiBr_6$/Au (free planar heterojunction device)	1.02	0.97	60	0.6	[69]
Spin coating	FTO/c-TiO_2/m-TiO_2/Li+$Cs_2AgBiBr_6$/Carbon	3.15	1.177	69.4	2.57	[70]
Spin coating-Antisolvent	ITO/CuNiO/$Cs_2AgBiBr_6$/C60/BCP/Ag	3.19	1.01	69	2.23	[71]
Spin coating	FTO/c-TiO_2/m-TiO_2/$Cs_2AgBiBr_6$/Spiro-OMeTAD/ Au	3.93	0.98	63	2.43	[12]
Spin coating	FTO/c-TiO_2/m-TiO_2/$Cs_2AgBiBr_6$/spiro-OMeTAD/ Ag	3.22	1.02	69.32	2.28	[72]
	FTO/*c*-TiO_2/m-TiO_2/C-Chl/$Cs_2AgBiBr_6$/spiro-OMeTAD/Ag	4.09	1.04	73.12	3.11	[72]
Solution Process	FTO/TiO_2/$Cs_2AgBiBr_6$/spiro-OMeTAD/MoO_3/Ag	0.1	0.65	38.4	0.028	[73]
Vacuum sublimation and Solution Process	FTO/TiO_2/$Cs_2AgBiBr_6$/Spiro-OMeTAD/MoO_3/Ag.	3.82	1.01	65	2.51	[45]
Spray coated	FTO/c-TiO_2/mp-TiO_2/$Cs_2AgBiBr_6$/SpiroOMeTAD/Au	3.1	1.091	70	2.3	[74]
Spin coating (Solvent annealing at 250 ∘C)	FTO/BL-TiO_2/*mp*-TiO_2 layer/perovskite/ Spiro-OMeTAD/Au	3.96	0.98	62.4	2.43	[66]
Spin coating- low pressure assisted (PEA Concentration = 6%)	PEDOT: PSS/$Cs_2AgBiBr_6$/PCBM/BCP/Al	2.76	1.06	1.02	1.78	[75]
Spin coating,	ITO/SnO_2/$Cs_2AgBiBr_6$/Siro-OMeTAD/Au	11.29	0.92	60.93	6.37	[32]
Hot injection	FTO/NiO/$Cs_2AgBi_{0.6}Sb_{0.4}Br_6$(NCs)/PCBM/Ag	1.07	0.275	31	0.09	[42]
Lithography	ITO/NiOx/$Cs_2AgBiBr_6$/PTAA/Au	—	—	—	2.84	[76]
Low-pressure assisted method	ITO/SnO_2/$Cs_2AgBiBr_6$/P3HT/Au	1.78	1.04	78	1.44	[69]
Spray coated	FTO/c &mp-TiO_2/$Cs_2AgBiBr_6$/Spiro-OMeTAD/Au	3.2	1.093	68	2.3	[44]
Spin coating Sol-gel method	FTO/TiO_2/ $Cs_2Ag_{0.95}Ga_{0.05}BiBr_6$ /Spiro-OMeTAD	6.01	0.94	80	4.52	[33]
Spin coating Sol-gel method	FTO/TiO_2/$Cs_2AgBiBr_6$/Spiro-OMeTAD/Au	5.13	0.92	73	3.48	[33]
Sol-gel Spin coating Method	FTO/TiO_2/$Cs_2Ag_{0.95}Al_{0.05}BiBr_6$/Spiro-OMeTAD/Au	5.29	0.91	71	3.40	[34]
Sol-gel Spin coating Method	FTO/TiO_2/$Cs_2AgBiBr_6$/Spiro-OMeTAD/Au	5.01	0.89	67	3.02	[34]
One step Spin coating Method	FTO/SnO_2/$Cs_2AgBiBr_6$/Carbon	1.71	0.69	47.9	0.54	[77]
Spray Coated	FTO/c-TiO_2/$Cs_2AgBiBr_6$/Carbon	—	1.29	30.0	0.19	[78]
Spray Coated	ITO/c-TiO_2/$Cs_2AgBiBr_6$/Spiro/Au	1.33	1.19	67.7	1.07	[79]
Spin coating	FTO/c-TiO_2/ $Cs_2AgBiBr_6$/PBDB-T/MoO_3/Ag	3.34	1.28	77.5	3.31	[80]
Spin coating	ITO/c&m-TiO_2/$Cs_2AgBiBr_6$/Spiro/Au	1.77	1.05	71.7	1.33	[79]
Spin coating	FTO/m-TiO_2/ $Cs_2AgBiBr_6$/SnS QDs/Carbon	3.74	1.02	51.0	1.95	[81]
Spin coating	FTO/c&m-TiO_2/$Cs_2AgBiBr_6$/Spiro/Ag	2.38	1.23	71.0	2.09	[82]
Spin coating	FTO/c&m-TiO_2/$Cs_2AgBiBr_6$/Spiro/Au	3.50	1.07	66.0	2.47	[83]
Spin coating	FTO/m-TiO_2/ $Cs_2(Ag_{1-x}Zn_x)$ $BiBr_6$/Carbon	4.23	1.00	51.0	2.16	[81]
Spin coating	FTO/c&m-TiO_2/ $Cs_2AgBiBr_6$/MoS_2/Carbon	6.12	1.10	62.0	4.17	[84]
Spin coating	FTO/c&m-TiO_2/$Cs_2AgBiBr_6$/Carbon	2.61	1.20	71.0	2.22	[85]
Solvothermal Spin Coating	FTO/c&m-TiO_2/ D149-$Cs_2AgBiBr_6$/Spiro/Ag	8.85	0.72	70.0	4.47	[86]
Spin coating	FTO/c&m-TiO_2/$Cs_2AgBiBr_6$/Carbon	2.82	1.18	67.6	2.25	[85]

chemical stability. Some substances may react with or catalyze the degradation of others. Extended exposure to any of the above conditions can lead to a gradual decline in chemical stability, even for initially stable substances.

The maximum energy transfer (E_T) from extremely energetic hydrogen radicals to the surface atom of $Cs_2AgBiBr_6$ should be considered to describe the chemical interaction between plasma gas and $Cs_2AgBiBr_6$ film [88].

$$E_T = \frac{2ME(E + 2mc^2)}{(m + M)^2c^2 + 2ME} \tag{1}$$

Here, M is the mass of the chemical components in $Cs_2AgBiBr_6$ m is the mass of the hydrogen atom; E is the kinetic energy of the entering plasma heated hydrogen radical; and c is the speed of light. The equation could be reduced as follows if the kinetic energy E is considerably less than mc^2 ($mc^2 = 9.40 \times 10^8$ eV for the hydrogen atom in equation (2)) [88].

$$E_T = E\frac{4Mm}{(m + M)^2} \tag{2}$$

On the other hand, atomic hydrogen concentration increasing into the $Cs_2AgBiBr_6$ lattice raises the formation energy of perovskite. Equation (3) can be used to compute the breakdown enthalpy for potential pathways to examine the HDP material's chemical stability [88].

$$\Delta H = 2E[AX] + E[BX] + E[B'X_3] - E[A_2BB'X_6] \tag{3}$$

The reported maximum kinetic energy measured in hydrogenated $Cs_2AgBiBr_6$ was 9.3 eV, a value substantially lower than mc^2. In $Cs_2AgBiBr_6$, it was therefore possible to infer from equation (3) that energy was transferred from the hydrogen radicals to the surface atoms. Using this information, it was possible to calculate the maximum energy transfer (E_T) to the surface atoms of Cs, Ag, Bi, and Br which are 0.28 eV, 0.34 eV, 0.18 eV, and 0.46 eV, respectively [32]. The results of the calculations show that $Cs_2AgBiBr_6$ chemical bonds are difficult to break during the low-temperature hydrogen plasma treatment. Moreover, with the minimum hydrogenation treatment time (less than 1200 s) the $Cs_2AgBiBr_6$ lattices are more stable. Figure 9(a) shows the decomposition or structural instability of hydrogenated $Cs_2AgBiBr_6$ appears after 1400 s hydrogenation treatment. The discrepancy between the compound ($A_2BB'X_6$) and the decomposed binary products is explained by the equation (3). If the decomposition energy is positive, then the material is more stable rather than negative. Hence, the decomposition energies (ΔH) of CsBr, AgBr, Cs_2AgBr_3, $CsAgBr_2$, and $Cs_3Bi_2Br_9$ are estimated to be positive, which is higher than $MAPbI_3$, suggesting a higher thermodynamic stability of $Cs_2AgBiBr_6$. In $Cs_2AgBiBr_6$, Pb^+ cations have been replaced by Ag^+ and Bi^{3+} cations, as they have enhanced Coulomb interaction energy which particularly induces more positive decomposition energy (0.38 eV) [29]. On the other hand, ΔH of the Iodide based Cs_2AgBiI_6 is negative ($\Delta H = -0.41$ eV), indicating Cs_2AgBiI_6 is unstable and may decompose spontaneously [89]. These techniques can be used to forecast the likelihood of successfully engineering the A, B, or X sites of novel $Cs_2AgBiBr_6$-based perovskites thin film utilizing new elements. Figure 9(b), the hydrogenated $Cs_2AgBiBr_6$ PSCs show outstanding stability at both RT and up to 85 °C [32]. These results could promote the practical application of hydrogenated $Cs_2AgBiBr_6$ PSC devices.

Figure 9(c) shows a weak PL peak at 1.87 eV. However, figure 9(c) inset, for low temperature (23 K) shows an intense and blue-shifted peak at 1.98 eV. To comprehend the final destiny of photogenerated carriers, figure 9(d) shows the time-resolved photoluminescence (PL) curve, which exhibits a rapid initial decline succeeded by a gradual decay [11]. Radiative and nonradiative recombination rates are added together using PL decay curves. Between single-crystal and powder samples, the long PL decay time of about 660 ns does not differ significantly, and it most likely indicates the fundamental recombination lifetime of the material. On the other hand, nonradiative carrier recombination is the predominant pathway, as indicated by the weak PL. Because of this, the radiative recombination lifetime ought to be far longer than 660 ns, and the PL decay traces approximately the nonradiative decay rate. Good photovoltaic performance is indicated by long carrier recombination lifetimes [11].

Additionally, $Cs_2AgBiBr_6$ has opened up new possibilities for energy-related photo-catalysis, which entails the generation of electrons and holes through photon absorption, chemical oxidation, and reduction reactions mediated by photo-induced electrons and holes, as well as charge separation and migration to the reaction sites. In 2020, Huang *et al* studied $Cs_2AgBiBr_6$ under various catalytic circumstances, such as strongly basic or acidic solutions and substantially reducing/oxidizing atmospheres, and found that $Cs_2AgBiBr_6$ exhibits improved operational chemical stability [90]. Li *et al* 2021 fabricated a multifunctional Ti_3C_2Tx/TiO_2 ETL for planar $Cs_2AgBiBr_6$ solar cells by doping MXene nanosheets into TiO_2 to increase the carrier extraction efficiency [91]. Since the electron conductivity and mobility of solution-processed compact TiO_2 layers are often low, the charge can build up at the interface or in ETL. Notably, Ti_3C_2Tx/TiO_2 ETL-based devices with $Cs_2AgBiBr_6$ solar cells maintain 93% of their initial PCE of 2.8% after 15 days in the ambient atmosphere under constant AM 1.5 G sunshine irradiation. $Cs_2AgBiBr_6$ solar cells may maintain 80% of its initial PCE after 60 days even at high

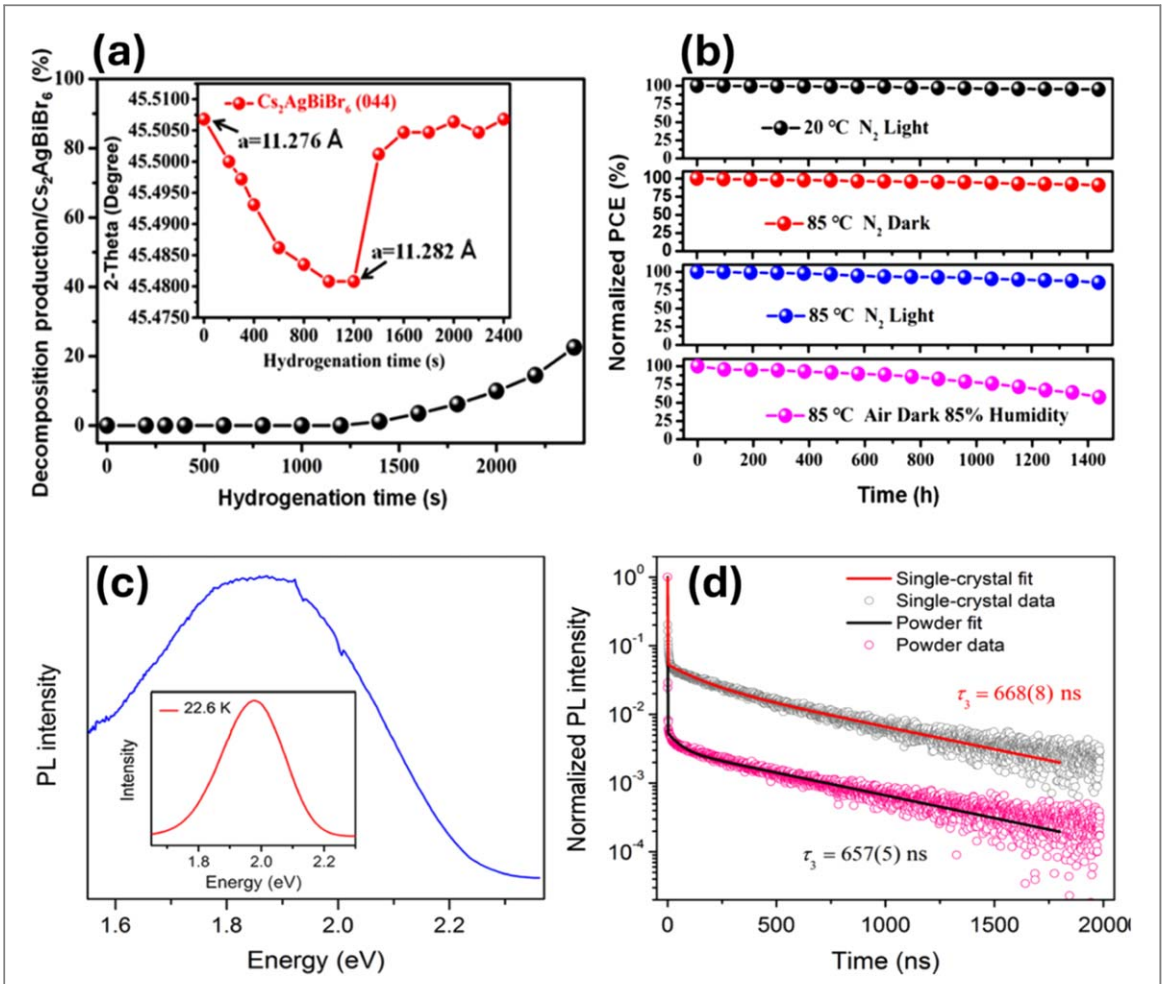

Figure 9. (a) The decomposition or intrinsic structural instability of hydrogenated $Cs_2AgBiBr_6$ appears after 1400 s hydrogenation treatment. (b) Normalized PCE (%) with different hydrogenation times under light illumination and nitrogen conditions at 85 °C. (Reproduced with permission from Zhang *et al* in 2022) [32]. (c) PL spectrum of a powdered sample in a steady state at room temperature after 500 nm excitation. Inset: PL at low-temperature (d) In powder and single-crystal samples, time-resolved room-temperature PL and fits for the PL decay time (τ) [11].

temperatures (85 °C, 0% RH). Table 3 shows the brief reported literature data on the chemical stability of different $Cs_2AgBiBr_6$ absorber layer-based PSCs.

3.2. Mechanical stability

Good mechanical stability in materials is influenced by various factors, and it is often a combination of factors rather than a single one. Some of the fundamental factors that contribute to good mechanical stability include Strong Chemical Bonds, Lattice Structure, Defects and Dislocations, Grain Size, Material Microstructure, Temperature and Environmental Effects, Crystal Symmetry, and Material Composition. Particularly, the type and strength of chemical bonds between atoms or molecules within a material play a crucial role in its mechanical stability. Also, the configuration of atoms or ions in a crystalline lattice can significantly impact mechanical stability. A well-ordered and tightly packed lattice structure can provide greater strength and stability to the material. The crystal structure and lattice parameters influence how a material responds to stress and strain. The existence of defects, such as vacancies, dislocations, or grain boundaries, can influence mechanical properties as well. While some defects can weaken a material, others can enhance its mechanical stability by acting as barriers to dislocation movement or providing toughening mechanisms. In polycrystalline materials, the grain distribution and size can have an impact on mechanical stability. Finer grain sizes often lead to improved mechanical properties, as they hinder the propagation of cracks and dislocations. The overall microstructure of a material, including the arrangement of different phases, can impact mechanical stability. Composite materials, for example, combine multiple phases to achieve specific mechanical properties. Importantly, mechanical stability can be temperature-dependent. Some materials may exhibit excellent stability at low temperatures but become brittle at elevated temperatures. The symmetry of a crystal structure can influence how a material responds to temperature stress. Anisotropic materials exhibit different mechanical properties in different directions, depending on their crystal symmetry. The type and proportion of elements or

Table 3. Reported chemical stability of $Cs_2AgBiBr_6$ absorber layer-based PSCs.

Structure	Efficiency	Stability	References
FTO/TiO_2/ $Cs_2AgBiBr_6$/PBDB-T	3.31% (98.5% of its original)	300 h	[80]
ITO/SnO_2/$Cs_2AgBiBr_6$/Spiro-OMETAD/Au	6.37%	1440 h (at 85 °C)	[32]
Ti_3C_2Tx/TiO_2 ETL for planar $Cs_2AgBiBr_6$	2.8% (93% of their initial value)	15 days	[76, 91]
$Cs_2AgBiBr_6$	80% of its original	60 days (at 85 °C)	[76, 91]
P3HT/ $Cs_2AgBiBr_6$ (65 nm)/Cu	1.91%	68days higher humidity	[92]
DP-150 $Cs_2AgBiBr_6$ NCs	—	240 days at ambient air, chemical	[17]
$Cs_2AgBiBr_6$ NCs	$Cs_2AgBiBr_6$ NCs could convert CO_2 into solar fuels like CO and CH_4, with total electron consumption of 10^5 μmolg^{-1}, with no H_2 side product	6 h	[93, 94]
Cs_2AgBiI_6 is greater than $Cs_2AgBiCl_6$	thermally stable	90 days (55% humidity)	[95]
$Cs_2AgBiBr_6$	Can tolerate light intensity of 70 mW cm^{-2} for 500 h	3 months	[96]
$Cs_2AgBiBr_6$ Superior thermal than $MA_2AgBiBr_6$	—	Several months	[97, 98]
$Cs_2AgBiBr_6$	—	14 days in dark condition	[11, 16]
$Cs_2AgBiBr_6$ and $Cs_2AgBiCl_6$	after exposed to halogen lamp radiation at 50 °C	30 days	[11]

compounds in a material can determine its mechanical properties. Alloying, for instance, can be used to tailor a material's mechanical stability.

Since the material will be subject to mechanical force during fabrication, understanding mechanical stability is essential. It should be emphasized that not every candidate HDP has a stable structure. A perovskite structure can be formed depending on (1) the octahedral factor (μ) and (2) the tolerance factor (t) [26]. Goldschmidt Tolerance Factor (GTF) is generally adopted for the calculation of the crystallographic stability of the HDP structure by t [27] and μ [28]. As seen in equations (4) and (5), GTF is a dimensionless empirical index that can forecast a perovskite's regular crystal structure.

$$\tau = \frac{r_A}{r_B} - n_A\left(n_A - \frac{r_A/r_B}{\ln\left(r_A/r_B\right)}\right) \tag{4}$$

$$\mu = \frac{r_A}{r_B} \tag{5}$$

Where n_A is the oxidation state, r_A, and r_B is the ionic radius of ions A and B, and $r_A > r_B$. For the case of HDPs consisting of two different cations then r_B represents the average radius of both B^+ and B^{3+} cations. To become a stable structure of a HDP, the GTF and Octahedral factor μ must be within $0.81 < t < 1.11$, and $0.41 < \mu < 0.90$, respectively [27]. In the case of $Cs_2AgBiBr_6$ HDP, GTF is $t = 0.890$, and the octahedral factor for the octahedron $[AgBr_6]^{5-}$ is $\mu = 0.587$ [28]. Moreover, the values of elastic constant, C_{11}, C_{12}, and C_{44} are necessary to assess for understanding the mechanical stability of the cubic system as shown in figure 10. There are a lot of experiments have be conducted focusing the material $A_2B^+B^{3+}X_6$ which have been exhibited well mechanical stability [100–102]. Furthermore, it is clear from figure 10 that $Cs_2AgBiBr_6$ exhibits anisotropic Poisson's ratio, Young's modulus, and Shear's modulus [99, 101–103].

The mechanical stability of Cs_2CuMCl_6 (M = Bi, and Sb) was recently analyzed by Nabi *et al* 2021. From table 4, the elastic parameters for Cs_2CuMCl_6 (M = Bi, and Sb) can be seen which indicating that the material is mechanical stable; as the C_{11}-values are found to be higher than C_{12} and C_{44} [103]. Since in this case, $C_{44} > 0$, C_{11}—$C_{12} > 0$, $C_{11}+2C_{12} > 0$, and other stability conditions are met, Yang *et al* demonstrated that $Cs_2AgBiBr_6$ is also mechanically stable [40]. In addition, the bulk modulus (B) is greater than the shear modulus (G), indicating that these systems are greater resistant to volumetric deformation than to shape deformation. The Poisson's ratio and Pugh's ratio of Cs_2CuMCl_6 are found to be higher than the critical value, i.e., 1.75 and 0.26, respectively, showing that these systems are ductile.

In summary, mechanical stability is a complex property influenced by multiple factors, including chemical bonding, lattice structure, defects, microstructure, temperature, and composition. The specific combination of these factors will vary depending on the material and its intended application. Achieving good mechanical stability often involves a careful balance of these factors to meet the desired performance requirements.

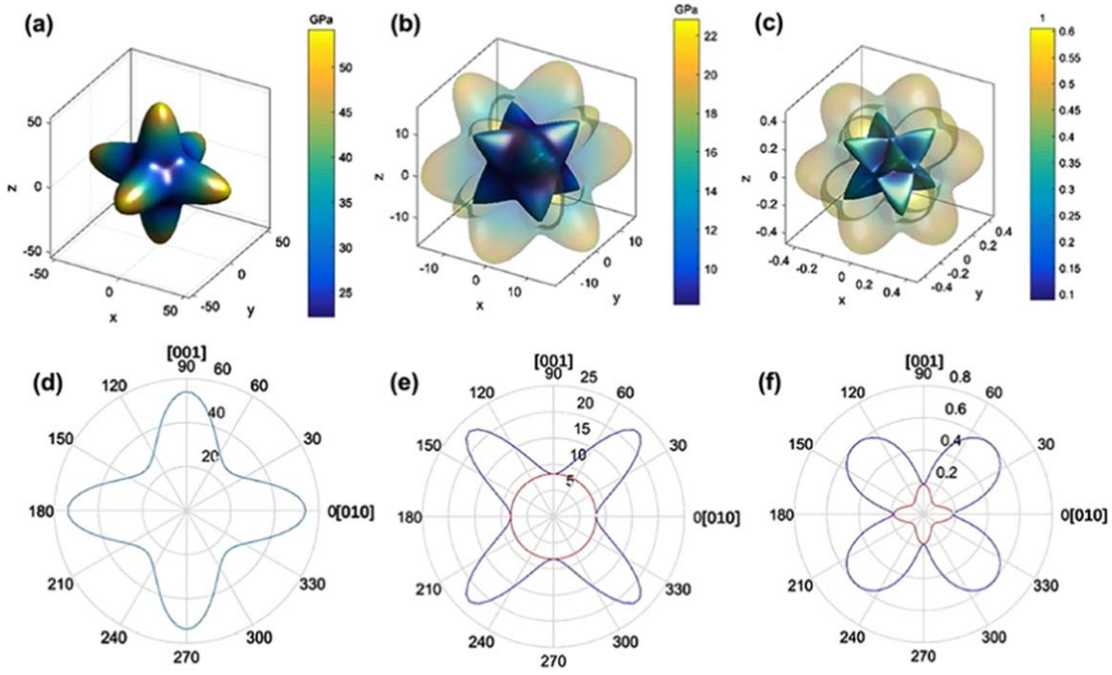

Figure 10. (a)–(c) and (d)–(f) Young's modulus(E), Shear modulus(G), and Poisson's ratios(ν) in 3D and 2D views for $Cs_2AgBiBr_6$, respectively. Reproduced with permission [99].

Table 4. 2nd order elastic constants (SOECs) for Cs_2CuMCl_6 (M = Sb, Bi) and $Cs_2AgBiCl_6$ achieved within the GGA-PBE framework by applying the energy-strain technique [103–105].

Parameters	$Cs_2CuSbCl_6$	$Cs_2CuBiCl_6$	$Cs_2AgBiCl_6$ [105]	$Rb_2AgGaCl_6$ [104]	$Rb_2AgGaBr_6$ [104]
C_{11}(GPa)	57.21	56.27	50.03	33.641	31.607
C_{12}(GPa)	19.56	19.23	19.96	30.858	28.225
C_{44}(GPa)	5.05	4.05	7.76	13.737	10.109
Young's modulus(Y)	32.86	21.77	27.35	24.167	18.787
Poisson's ratio(σ)	0.32	0.38	0.35	0.373	0.393
Deby temp. (Θ_D in K)	151.17	133.38	164	—	—
Bulk modulus(B in GPa)	32.11	31.57	29.98	31.786	29.352
Shear Modulus (B in GPa)	12.36	7.86	10.14	—	—
Pough's ratio (B/G)	2.59	4.01	2.96	3.61	4.35

3.3. Thermal stability

Thermal stability in the context of PSCs refers to the ability of the perovskite material used in the solar cell to maintain its structural and electronic properties at elevated temperatures over an extended period. When exposed to high temperatures, perovskite materials can degrade, leading to decrease of device performance and a shortened the operational lifespan. To identify the thermal stability of a perovskite material in a fundamental manner, researchers typically perform a series of experiments and analyses, looking for specific indicators and changes in the material's properties. Here we briefly discussed some key factors and techniques used to assess thermal stability:

Particularly, researchers often subject the perovskite material to a range of temperatures and monitor various properties such as crystallinity, morphology, and electrical performance. This involves heating the material gradually and characterizing its response at different temperature intervals and the PL spectroscopy is utilized to measure the material's light emitting capability after it absorbs photons. Changes in the PL spectrum can indicate defects and degradation in the perovskite material, providing insights into its thermal stability. Also, several researchers conduct accelerated aging tests where perovskite solar cells or films are subjected to high temperatures for an extended period. Monitoring the changes in efficiency, voltage, and current output over time helps to assess how the material's performance degrades. Thermogravimetric analysis (TGA) and differential scanning calorimetry (DSC) can also be used to reveal details of thermal behavior and breakdown of perovskite materials.

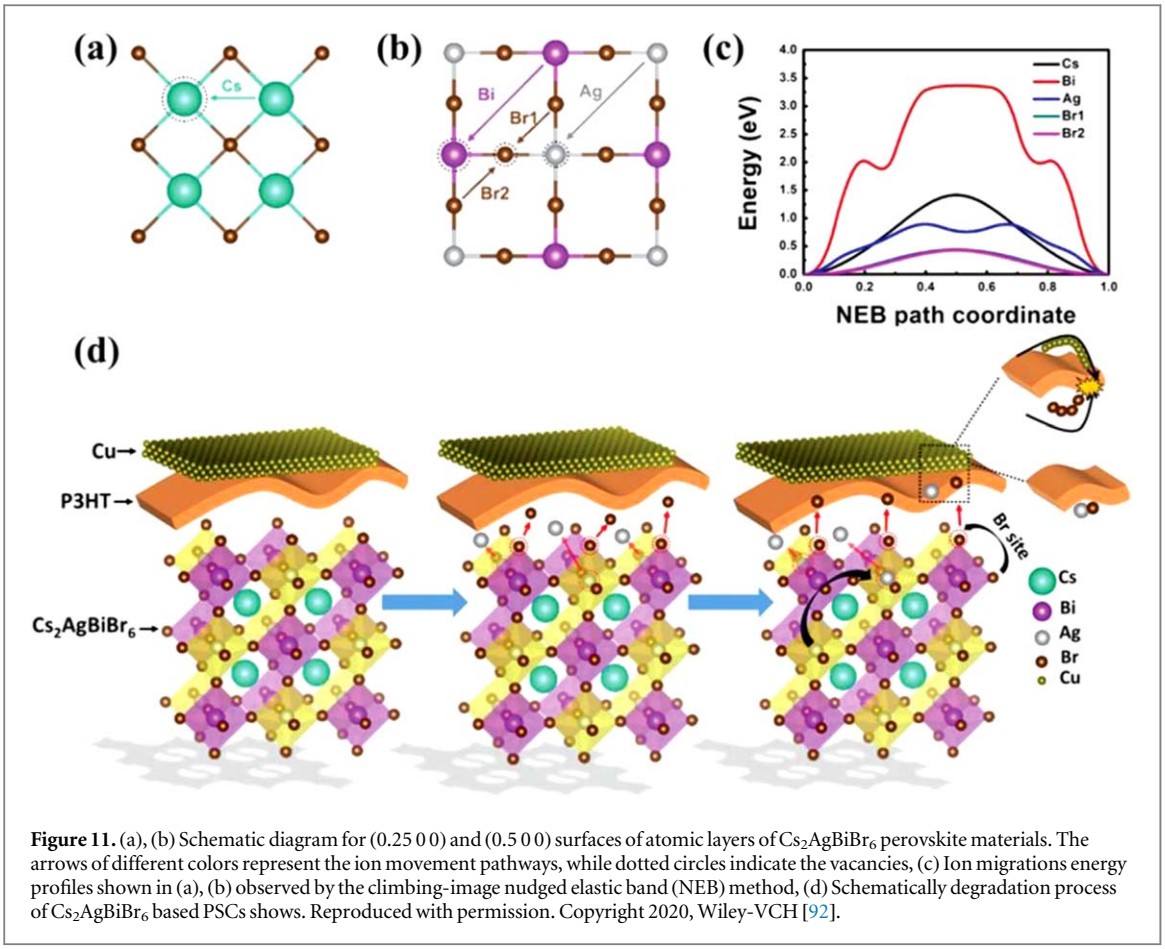

Figure 11. (a), (b) Schematic diagram for (0.25 0 0) and (0.5 0 0) surfaces of atomic layers of $Cs_2AgBiBr_6$ perovskite materials. The arrows of different colors represent the ion movement pathways, while dotted circles indicate the vacancies, (c) Ion migrations energy profiles shown in (a), (b) observed by the climbing-image nudged elastic band (NEB) method, (d) Schematically degradation process of $Cs_2AgBiBr_6$ based PSCs shows. Reproduced with permission. Copyright 2020, Wiley-VCH [92].

The goal of these fundamental assessments is to help us to determine the temperature at which the perovskite material begins to degrade, the rate of degradation, and the mechanisms involved. Understanding these aspects is crucial for designing more stable perovskite solar cells and improving their long-term reliability for practical use in renewable energy applications. According to Dong *et al* in 2018, $Cs_2AgBiBr_6$ has superior thermal stability than $MA_2AgBiBr_6$ [97]. It preserves phase purity for several months [98]. Moreover, the stability of Cs_2AgBiI_6 is greater than $Cs_2AgBiCl_6$ [106]. $Cs_2AgInCl_6$ is thermally stable for 90 days under the presence of 55% humidity. $Cs_2AgInCl_6$ point defects have been observed by Xu *et al* and their existence degrades the electronic property, impairing the performance of the photocatalytic reaction [96]. However, by modifying the growing conditions, defects can be reduced. According to Cai *et al* $Cs_2GeMnBr_6$ is unstable at 0 K because soft phonon mode is present, but it is determined to be stable at room temperature (RT) because soft phonon mode is absent. For instance, Filip *et al* found that only three out of 18 variants of the chemical compound $Cs_2B^+B^{3+}X_6$ with B^+ = Cu, Ag, Au; B^{3+} = Bi, Sb; and X = Cl, Br, I are stable under elevated thermal conditions [12, 57, 107–109].

At RT, $Cs_2AgBiBr_6$ typically crystallizes in a space group of fm3m with an fcc structure, but when the temperature is lowered, the material's dimensions are changed, it is subjected to high-pressure treatment or new doping elements are added to the lattice, phase transitions may occur. For instance, at RT, the tetragonal phase (space group I4/m) will develop at 122 K or high pressure of around ≈2.3 GPa from the cubic phase at that temperature [95]. Reduced symmetry in the octahedra results in a similar phase change when a specific amount of Fe takes the place of Bi in the lattice [110]. The optoelectronic properties as well as thermal stability of hydrogenated $Cs_2AgBiBr_6$ PSCs have been effectively improved after hydrogenation treatment. These results could promote the practical application of hydrogenated $Cs_2AgBiBr_6$ PSC devices.

Particularly, the device's stability is seriously jeopardized by the ion migration phenomenon. In 2020, Ghasemi *et al* noted that in comparison to Ag and Br, the Bi ion has a higher ion-migration energy barrier (3.363 eV) and larger ionic radii, which reduce its ability to migrate [92]. Interestingly, Ag+ and Br− ions can accumulate between the P3HT layer and the metal contact by diffusing in the same direction, as shown in figures 11(a), (b). This is corroborated by experimental observations, as shown in figure 11(c), of accelerated degradation of the Cu metal electrode and the $Cs_2AgBiBr_6$ thin film in devices based on thin P3HT layers. In these devices, from figure 11(d), the inhomogeneous P3HT increases the likelihood of direct contact between Cu and the $Cs_2AgBiBr_6$ thin film, which causes the device and perovskite layer to deteriorate much more quickly. Fortunately, this degradation process can be effectively mitigated by using a thicker P3HT layer. Furthermore, it

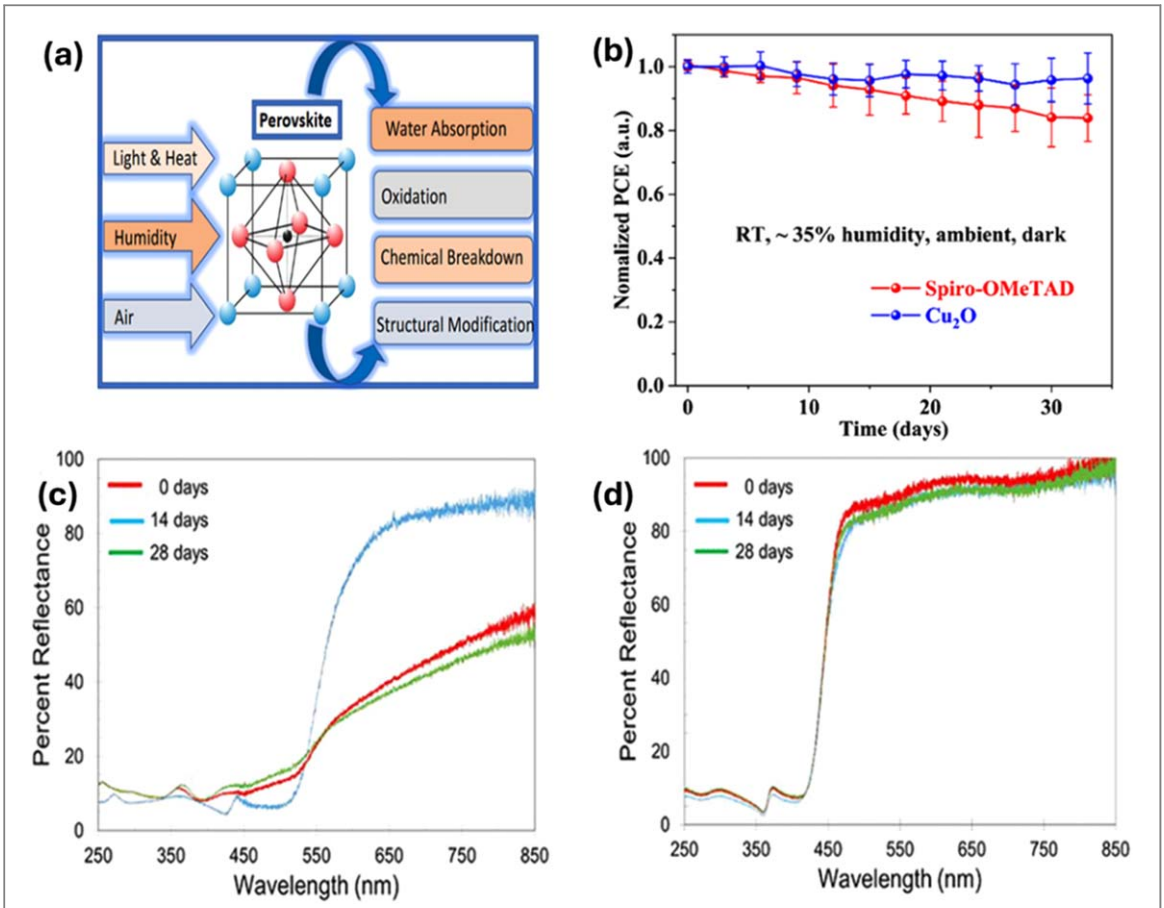

Figure 12. (a) Schematics for degradation factors of perovskite material due to environmental factors (b) comparison of the stability of the $Cs_2AgBiBr_6$ PSCs between Spiro-OMeTAD and Cu2O HTLs [111]. (Reproduced with permission from Xiao et. Al. in 2021. (c)–(d) The $Cs_2AgBiBr_6$ and $Cs_2AgBiCl_6$ UV-vis spectra were obtained after 14 and 28 days, respectively [16]. (Reproduced with permission from McClure *et al* in 2016).

was discovered that conductivity was influenced by HTL's thickness also [111]. The long-term stability of lead halide perovskite solar cells has been demonstrated to be improved by suppressing ion migration. This includes interfacial engineering on the surface of the perovskite layer/HTL grain boundaries and chemical bonding enhanced immobilization of cations and anions [111–113]. Similar technique could be utilized to improve the Cs-based HDP PSCs.

3.4. Light and moisture stability

Light stability refers to the ability of a material, in this case, $Cs_2AgBiBr_6$ perovskite, to maintain its performance and structural integrity when exposed to various types of light, especially sunlight. Perovskite solar cells absorb sunlight to generate electrical energy, but prolonged exposure to light can cause degradation through the defects formation or the breakdown of the perovskite crystal structure. Light stability is crucial because it determines the long-term performance and durability of the solar cell. In the context of $Cs_2AgBiBr_6$ perovskite solar cells, researchers and engineers aim to develop materials and device designs that can withstand extended exposure to sunlight without significant degradation. Achieving good light stability is a key challenge in advancing the commercial viability of perovskite solar technology. Moisture stability, also known as water stability, refers to the ability of a perovskite solar cell to resist the detrimental effects of moisture or humidity. Perovskite materials are generally sensitive to water, as exposure to moisture can lead to rapid degradation, such as the formation of hydrates or the decomposition of the perovskite structure. This sensitivity makes moisture stability a critical concern for PSCs, especially in real-world outdoor environments. $Cs_2AgBiBr_6$-based PSCs need to be protected from moisture to ensure their performance for a long time and reliability. Methods of encapsulation are being developed by researchers and moisture-resistant materials to shield the perovskite layer from environmental factors like rain, humidity, and dew. Figure 12(a) shows the schematic diagram of the degradation factors for decomposing of the PSCs by influence by ambient conditions.

All-inorganic $Cs_2AgBiBr_6$ has inherently show high stability against light and moisture. However, stability problems arise for practical devices incorporating organic interlayers. In solar cells, anomalous ion movement of Ag and Br from $Cs_2AgBiBr_6$ to P3HT/Cu interface is seen after 68 days of storage at higher humidity, which may

be a result of the halide's volatility or reactivity with Ag or Cu metals [92]. Therefore, more research is required to identify the probable degradation pathways for $Cs_2AgBiBr_6$ PSCs using organic materials, like constant illumination of light, to provide a high level of stability for practical use. Klarbring, *et al* in 2020 showed that chemical linkages do not break down in crystals for up to 240 days when they are exposed to ambient air [17]. Their findings show that after a hydrogen plasma treatment, it is difficult to break the chemical bonds in $Cs_2AgBiBr_6$. The $Cs_2AgBiBr_6$ lattice, however, is only stable while the hydrogenation treatment is under 1200s. The degradation of the hydrogenated $Cs_2AgBiBr_6$ phase occurs higher than 1400 s hydrogenation treatment, which is due to the hydrogenated $Cs_2AgBiBr_6$ inherent structural instability. The formation energy of perovskite increases as the amount of atomic hydrogen present in $Cs_2AgBiBr_6$ [32]. Xiao et al 2021 reported a straightforward and practical method for effective inorganic HTLs towards enhancing the PCE, and enhancing the stability of lead-free, all-inorganic perovskites. In a closed test box without encapsulation and with 35% relative humidity, the stability of both Cu_2O and Spiro-OMeTAD-based devices was also compared. As shown in figure 12(b), it continues to retain over 96% of its initial PCE after 33 days in an atmospheric environment (room temperature and 35% of relative humidity) for Cu_2O HTL. Same study reported that the PCE of only 84% retained for the same duration for the device that uses Spiro-OMeTAD HTL [111]. This suggests that the $Cs_2AgBiBr_6$ film, which is based on Cu_2O, performs fairly steadily in terms of high humidity and temperature.

Several studies have shown that $A_2B^+B^{3+}X_6$ are more stable under ambient conditions. The stability of Cs_2AgBiX_6 (X = Cl, Br) has been examined in a dark and light environment. This observation exhibited that the material is stable for 14 days in a dark condition [16]. Figure 12(c) shows that $Cs_2AgBiCl_6$ undergoes minimum degradation for up to 14 days, on the other hand, $Cs_2AgBiBr_6$ showed extreme degradation [16]. According to Zhou *et al* (2018), $Cs_2AgBiCl_6$ nanocrystals can tolerate the light intensity of 70 mW cm^{-2} for 500 h and maintain its phase stability for up to three months in the presence of 55% of relative humidity [96].

The stability of $Cs_2AgBiBr_6$ powder in the presence of light and humidity has been studied by Slavney *et al* The UV-Vis spectra in figure 12(d) makes it evident that $Cs_2AgBiBr_6$ can be stable in the dark for up to a month, however, discoloured after being exposed to light for 15 days [11]. It has been reported that the photosensitivity of Ag salt could be responsible for this discoloration [39]. Additionally, crystals heated at 100 °C for 72 h or exposed to halogen lamp radiation at 50 °C for 30 days showed no signs of breakdown, and mass loss was only seen at above 430 °C temperature [11]. The stability of the solar cell devices are eventually impacted by the device architecture. The Planar and Scaffold devices were contrasted in a similar controlled environment. Researchers and engineers are actively working to increase the stability of PSCs through various strategies, including the development of better encapsulation techniques, more stable perovskite compositions, and novel device architectures. Achieving higher stability is a key milestone on the way to the widespread adoption of perovskite solar cells as a clean and efficient energy source.

4. Challenges of Pb-free HDP solar cell

Tunable absorption-emission across the entire visible and ultraviolet spectrum and high stability attract significant research interest. Also, a vast number of possible HDP materials have attracted the researchers; however, many of them are yet to be synthesized. In the following sections, we are analyzing some other challenges for HDP-based PSCs. According to the SQ limit for a solar cell, the perfect bandgap range for the material is around 1.1 to 1.4 eV [114]. Unfortunately, the bandgap of Cs-based HDPs are above 2.0 eV which can be reduced to 1.9 eV via doping and the theoretical S-Q limit efficiency could be 25%. The primary cause is that the higher band gap will makes electron leaping more challenging, which indicates the inherent restriction of weak light absorption. Consequently, to increase the photocurrent of $Cs_2AgBiBr_6$ PSCs, bandgap (E_g) modulation is required, such as band gap narrowing or the shift from indirect to direct [115]. However, the majority of reported HDPs exhibit extremely wide bandgaps which are greater than 2.2 eV which makes it inappropriate for absorber layers in the case of PSCs. The bandgap could be reduced using a variety of methods, including the inclusion of metal cations such as Tl, Sb, Mn, Na, K, Li, In, Al, and Ga etc, which lowers the bandgap by up to 1.6 eV. However, due to the toxic issues, thallium doping is excluded from the research scope. In-based HDPs $Cs_2AgInCl_6$ is a direct bandgap material with ~1.6 μs of carrier lifetime [15]. However, these HDPs are not a suitable candidate for optoelectronic application due to its only 1.6% Photoluminescence Quantum Yield (PLQY), and large bandgap. This low PLQY can be increased up to 16% by Mn doping with the HDP $Cs_2AgInCl_6$, but it is still not a suitable amount for application [116]. On the other hand, the trivalent Sb doped $Cs_2AgSbCl_6$ HDPs has an indirect bandgap of 2.54 eV, which arises because of the conduction band maximum contribution of its 5p orbital, and $Fm\bar{3}m$ space group [117]. The bandgap may be lowered by alloying using Sb^{3+}, however, the synthesis of Sb-rich alloys is challenging because $Cs_2AgSbBr_6$ has a large bandgap of its own, and require high formation energy. As the Bi and Sb have quite similar ion pair activity and almost same atomic size of about 90 pm, by inclusion of both these materials can reduce Cs_based HDPs optical bandgap

from 2.0 eV to 1.6 eV and increase the stability of the HDP layer as well [118]. Moreover, Sb incorporation introduces a bandlike charge transport mechanism (depending on temperature) which is similar to the Pb-based perovskites and showed red shift [119]. Hence, Sb may be the best possible solution to dope with Bi due to its similar ion pair activity. On the other hand, most recently Ihtisham et al in 2024, were able to reduce the band gap from 1.91 eV to 1.86 eV by Ga doping perovskite layer [33]. Consequently, the overall PCE increased from 3.51% to 4.52%, which shows a significant improvement over the pure $Cs_2AgBiCl_6$ HDP solar cell. Asad et al in 2024, were able to lower the band gap from 1.91 eV to 1.82 eV by Al doping with perovskite layer $Cs_2AgBiBr_6$. The J-V curve indicates that the pure $Cs_2AgBiCl_6$ HDP PSC had an efficiency of 3.02%, a Voc of 0.89 V, FF of 0.67, and Jsc of 5.01 mA cm^{-2}. Improvements were seen when Al was doped; Voc increased to 0.91 V, FF to 0.71, and Jsc to 5.29 mA cm^{-2}. As a result, the overall PCE increased to 3.40%, a significant 12.5% improvement over the pure PSCs [34].

Direct bandgap In and Tl-based HDPs are challenged by parity-forbidden transitions. Photon energy near the bandgap is weakly absorbed by the parity-forbidden transitions, which is not desirable for thin-film applications. The parity-forbidden transition is frequently broken by doping or alloying at high concentrations [120]. The low PLQY of HDPs is one of their main disadvantages. The goal of several groups has been to raise the PLQY of HDP. By suppressing the surface defect, doping with an additional metal ion, or adding water during synthesis can occasionally lead to an increase in the PLQY of HDP [20]. HDP typically has a stable cubic structure, however occasionally; the orbital interaction is restricted by the cubic unit cell, resulting in a large bandgap and a narrow conduction band edge. Further study of charge carrier dynamics is crucially needed to comprehend the charge transfer mechanism also [121]. Halide perovskites' morphology, or their size and shape, could be readily adjusted, however, tuning the morphology of HDPs remains yet challenging task [122].

To form HDP, need to precisely control the amounts or ratio of the precursor materials. Moreover, component engineering might be feasible through the alloying of rare earth elements, which might result in a notable alteration in optical characteristics. The construction of the device presents certain hurdles because of the high temperatures needed to prepare certain HDPs. One of the primary obstacles to quickly gaining a thorough grasp of this class of materials is the solubility of the precursors [123]. Solution-processed HDPs are more difficult to fabricate than lead halide perovskites due to several issues. More precursors are required, and most halide salts are poorly soluble in the solvents. One way to solve this problem might be to use solid-state synthesis methods (like ball-milling powder synthesis).

5. Future scope and conclusion

PSCs' performance has greatly increased in recent years, and they are currently thought to be a great alternative to silicon solar cells. However, the development of innovative, affordable fabrication techniques is required to support the commercialization. Furthermore, the industrial promotion and development of PSCs will be impeded by the severe hazard of the Pb element employed in PSCs. Instead of Pb, nontoxic Cs-based HDPs could be a better substitute for the future commercialization. In this paper, we have described several approaches to improve the performance of Pb-free halide double PSCs, including the use of different fabrication procedures and stability concerns. It is evident that significant obstacles still exist despite a great deal of study into the development of Cs based Pb free PSCs. Although the solution process is the foundation of most current perovskite material synthesis techniques, alternate synthesized approaches to the solution process must be developed. It should be mentioned that as a single junction solar cell application, efficiency levels of Cs-based halide double PSCs are below 7% that are not suitable for commercialization. We think that the precise recombination and charge carrier dynamics of $Cs_2AgBiBr_6$ remain a matter of great scientific debate and efficiency could be improved via solving the critical issues belongs to the material and device. The future prospective and different challenges for the $Cs_2AgBiBr_6$ base can be seen in figure 13:

The only effective option is increasing efficiency would be modifying the energy bandgap and/or type of the bandgap by utilizing novel synthesizing technique, and/or doping to $Cs_2AgBiBr_6$. Appropriate elemental doping strategies must be investigated in order to successfully tune the bandgap. Up till now, this problem has not been resolved by the trade-offs associated with replacing the Ag or Bi elements which can be try in future. Direct bandgaps can be substituted for indirect ones, giving optoelectronic properties, with low-dimensional derivatives of $Cs_2AgBiBr_6$ offering these opportunities. Since it has a considerable impact on carrier scattering, charge carrier mobility, photoluminescence linewidth broadening, photoluminescence quantum yields, and electron-hole recombination, strong electron-phonon coupling is a major issue for $Cs_2AgBiBr_6$ double perovskite. To fully comprehend changes to the electron-phonon coupling in $Cs_2AgBiBr_6$, more research is required. The decreased electron-phonon coupling in $Cs_2AgBiBr_6$ appears to be achievable through several methods, such as doping/alloying, hetero-junction structures, dielectric confinement, and bond length compression. The decreased coupling between electrons and phonons will greatly boost current density, which

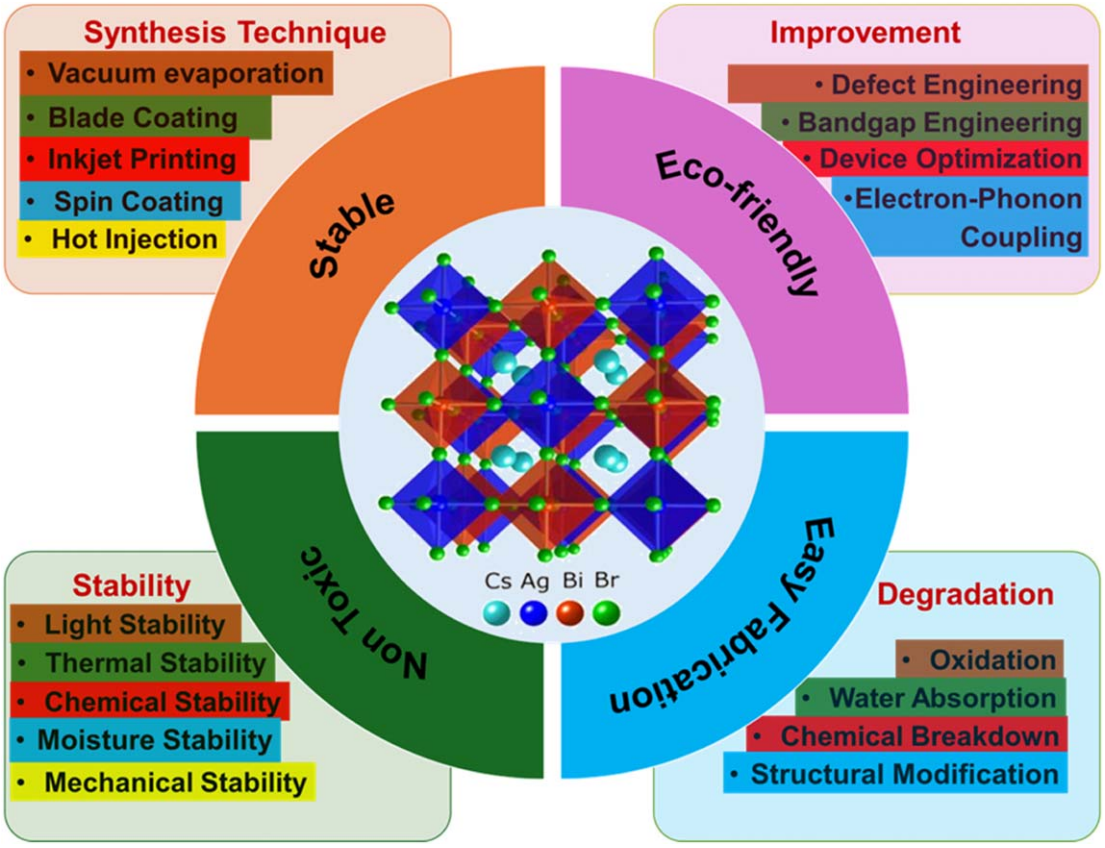

Figure 13. Future prospective and different challenges.

subsequently improves light response as well as the device efficiency. To lessen non-radiative recombination, it is advisable to avoid the potential antisite defects (BiAg or AgBi) and vacancy defects (Br or Bi vacancies). Experimental evidence is required to analyze, how defects affect the performance of devices and the material's optoelectronic capabilities. To lessen deep-level defects, growth condition optimization strategies, the addition of passivation materials, or changes to device interfaces have to investigate in details. Importantly, various simulations result shows higher PCE (more than 18%) of $Cs_2AgBiBr_6$ as an absorber layer, thus we believe that there is a great opportunity to increase the efficiency by applying pre- and post-crystallization techniques as well as via solving above mentioned factors belongs to the materials and devices.

Acknowledgments

This work was supported by the Malaysian Ministry of Higher Education through FRGS grant FRGS/1/2020/TK0/UM/02/33. The authors also acknowledge the support from the Faculty of Engineering, Universiti Malaya (@UM).

Conflicts of interest

Authors declare that there has no conflict of interest. All authors have read and agreed to the published version of the manuscript.

Data availability statement

All data that support the findings of this study are included within the article (and any supplementary files).

ORCID iDs

Hairul Mardiah Hamzah https://orcid.org/0000-0003-3557-7259
Suhana Mohd Said https://orcid.org/0000-0001-5258-9070

S F W M Hatta https://orcid.org/0000-0001-9519-073X
Mohammad Aminul Islam https://orcid.org/0000-0002-3862-9125

References

[1] Kothandapani Z, Islam M A, Reza Y, Hasan A A Q, Alkahtani A A and Amin N 2020 Optimization of Cu2O and CUSCN as HTL of planar perovskite solar cells via numerical simulation *Journal of Ovonic Research* **16** 369–77
[2] Green M A 2024 Solar Cell Efficiency Tables (Version 65) *Progress in Photovoltaics: Research and Applications* (https://doi.org/10.1002/pip.3867)
[3] Wang R, Mujahid M, Duan Y, Wang Z K, Xue J and Yang Y 2019 A review of perovskites solar cell stability *Adv. Funct. Mater.* **29** 1–25
[4] Wang R, Wang J, Tan S, Duan Y, Wang Z-K and Yang Y 2019 Opportunities and challenges of lead-free perovskite optoelectronic devices *Trends Chem* 1–12
[5] Jiang Y *et al* 2019 Reduction of lead leakage from damaged lead halide perovskite solar modules using self-healing polymer-based encapsulation *Nat. Energy* **4** 585–93
[6] Li X, Zhang F, He H, Berry J J, Zhu K and Xu T 2020 On-device lead sequestration for perovskite solar cells *Nature* **578** 555–8
[7] Zhang Y Y 2018 Intrinsic instability of the hybrid halide perovskite semiconductor CH3NH3PbI3 *Chinese Physics Letter* **35** 036104
[8] Kung P K *et al* 2020 Lead-free double perovskites for perovskite solar cells *Sol. RRL* **4**
[9] Obada D O, Abolade S A, SK R, Ukpong A M and Akande A 2023 Ab initio calculations of the properties of defective CsSnCl3: the role of anion-cation pair defect *Solid State Ion* **399**
[10] Hossain A, Bandyopadhyay P and Roy S 2018 An overview of double perovskites A2B′B″O6 with small ions at a site: synthesis, structure and magnetic properties *J. Alloys Compd.* **740** 414–27
[11] Slavney A H, Hu T, Lindenberg A M and Karunadasa H I 2016 A bismuth-halide double perovskite with long carrier recombination lifetime for photovoltaic applications *J. Am. Chem. Soc.* **138** 2138–41
[12] Greul E, Petrus M L, Binek A, Docampo P and Bein T 2017 Highly stable, phase pure Cs2AgBiBr6 double perovskite thin films for optoelectronic applications *J. Mater. Chem. A Mater.* **5** 19972–81
[13] Chen Z *et al* 2021 Processing and preparation method for high-quality opto-electronic perovskite film *Front Mater* **8** 1–13
[14] Lin C, Zhao Y, Liu Y, Zhang W, Shao C and Yang Z 2021 The bandgap regulation and optical properties of alloyed Cs2NaSbX6 (X = Cl, Br, I) systems with first principle method *Journal of Materials Research and Technology* **11** 1645–53
[15] Volonakis G J *et al* 2016 Lead-free halide double perovskites via heterovalent substitution of noble metals *J. Phys. Chem. Lett.* **7** 1254–9
[16] McClure E T, Ball M R, Windl W and Woodward P M 2016 Cs2AgBiX6 (X = Br, Cl): new visible light absorbing, lead-free halide perovskite semiconductors *Chem. Mater.* **28** 1348–54
[17] Ji F *et al* 2020 Lead-free halide double perovskite Cs2 AgBiBr6 with decreased band gap *Angew. Chem. Int. Ed.* **59** 15191–4
[18] Volonakis G *et al* 2017 Cs2InAgCl6: a new lead-free halide double perovskite with direct band gap *J. Phys. Chem. Lett.* **8** 772–8
[19] Zhang Y 2022 YSYLZZYWYYQDYYPQFH. thermochromic Cs2AgBiBr6 single crystal with decreased band gap through order-disorder transition *Small* **18** 2201943
[20] Longo G, Mahesh S, Buizza L R V, Wright A D and Alexandra J 2020 Understanding the performance limiting factors of Cs 2 AgBiBr 6 double-perovskite solar cells *ACS Energy Lett.* **5** 2200–7
[21] Ning W *et al* 2018 Long electron–hole diffusion length in high-quality lead-free double perovskite films *Adv. Mater.* **30** 1–6
[22] Schade L *et al* 2019 Structural and optical properties of Cs 2 AgBiBr 6 double perovskite *ACS Energy Lett.* **4** 299–305
[23] Biega R I, Filip M R, Leppert L and Neaton J B 2021 Chemically localized resonant excitons in silver-pnictogen halide double perovskites *J. Phys. Chem. Lett.* **12** 2057–63
[24] Hoye R L Z *et al* 2018 Fundamental carrier lifetime exceeding 1 μ s in Cs 2 AgBiBr 6 double perovskite *Advance Materials Interfaces* **5** 2–9
[25] Lei H, Hardy D and Gao F 2021 Lead-free double perovskite Cs2AgBiBr6: fundamentals, applications, and perspectives *Adv. Funct. Mater.* **31**
[26] Gao Y, Pan Y, Zhou F, Niu G and Yan C 2021 Lead-free halide perovskites: a review of the structure-property relationship and applications in light emitting devices and radiation detectors *J. Mater. Chem. A Mater.* **9** 11931–43
[27] Gold Schmidt V M 1926 Norsk geologisk tidsskrift 27 *Naturwissenschaften* **14** 477
[28] Li C, Lu X, Ding W, Feng L, Gao Y and Guo Z 2008 Formability of ABX 3 (X = F, Cl, Br, I) halide perovskites *Acta Crystallogr.* B **64** 702–7
[29] Savory C N, Walsh A and Scanlon D O 2016 Can pb-free halide double perovskites support high-efficiency solar cells? *ACS Energy Lett.* **1** 949–55
[30] Pai N *et al* 2020 Enhancement of the intrinsic light harvesting capacity of Cs2AgBiBr6 double perovskite: Via modification with sulphide *J. Mater. Chem. A Mater.* **8** 2008–20
[31] Islam M T *et al* 2021 Investigation of non-Pb all-perovskite 4-T mechanically stacked and 2-T monolithic tandem solar devices utilizing SCAPS simulation *SN Appl. Sci.* **3** 1–12
[32] Zhang Z *et al* 2022 Hydrogenated Cs2AgBiBr6 for significantly improved efficiency of lead-free inorganic double perovskite solar cell *Nat. Commun.* **13** 1–12
[33] Ihtisham-Ul-haq N *et al* 2024 Bandgap reduction and efficiency enhancement in Cs2AgBiBr6 double perovskite solar cells through gallium substitution *RSC Adv.* **14** 5440–8
[34] Ullah A, Iftikhar Khan M, Ihtisham-Ul-Haq N, Almutairi B S, Dalil D B and Choi J 2024 Bandgap engineering and enhancing optoelectronic performance of a lead-free double perovskite Cs2AgBiBr6 solar cell via al doping *ACS Omega* **9** 18202–11
[35] Huang J, Xiang H, Ran R, Zhou W, Wang W and Shao Z 2024 Fundamental understanding in the performance-limiting factors of Cs2AgBiBr6-based perovskite photovoltaics *Renew. Sustain. Energy Rev.* **191**
[36] Zhai M, Chen C and Cheng M 2023 Advancing lead-free Cs2AgBiBr6 perovskite solar cells: challenges and strategies *Sol. Energy* **253** 563–83
[37] Tress W and Sirtl M T 2022 Cs2AgBiBr6 double perovskites as lead-free alternatives for perovskite solar cells? *Sol. RRL* **6**
[38] Chand Yadav S, Srivastava A, Manjunath V, Kanwade A, Devan R S and Shirage P M 2022 Properties, performance and multidimensional applications of stable lead-free Cs2AgBiBr6 double perovskite *Mater. Today Phys.* **26** 100731

[39] Sk M 2022 Recent progress of lead-free halide double perovskites for green energy and other applications *Appl. Phys. A Mater. Sci. Process.* **128**
[40] Yang X, Wang W, Ran R, Zhou W and Shao Z 2020 Recent advances in Cs2AgBiBr6-based halide double perovskites as lead-free and inorganic light absorbers for perovskite solar cells *Energy Fuels* **34** 10513–28
[41] Ono L K, Leyden M R, Wang S and Qi Y 2016 Organometal halide perovskite thin films and solar cells by vapor deposition *J. Mater. Chem. A Mater.* **4** 6693–713
[42] Kumar A, Swami S K, Rawat S S, Singh V N, Sinha O P and Srivastava R 2021 Mixed bismuth-antimony-based double perovskite nanocrystals for solar cell application *Int. J. Energy Res.* **45** 16769–80
[43] Mathies F, Eggers H, Richards B S, Hernandez-Sosa G, Lemmer U and Paetzold U W 2018 Inkjet-printed triple cation perovskite solar cells *ACS Appl. Energy Mater.* **1** 1834–9
[44] Daem N *et al* 2021 Spray-coated lead-free Cs2AgBiBr6 double perovskite solar cells with high open-circuit voltage *Sol. RRL* **5**
[45] Igbari F *et al* 2019 Composition stoichiometry of Cs 2 $AgBiBr_6$ films for highly efficient lead-free perovskite solar cells *Nano Lett.* **19** 2066–73
[46] Sirtl M T *et al* 2020 Optoelectronic properties of $Cs_2AgBiBr_6$ thin films: the in fl uence of precursor stoichiometry *American Chemical Society* **3**
[47] Fan P *et al* 2016 High-performance perovskite $CH_3 NH_3 PbI_3$ thin films for solar cells prepared by single-source physical vapour deposition *Sci. Rep.* **6** 1–9
[48] Fan P, Peng H, Zheng Z, Chen Z, Tan S and Chen X 2019 Single-source vapor-deposited Cs2 AgBiBr6 thin films for lead-free perovskite solar cells *Nanomaterials* **6** 1–13
[49] Wang M *et al* 2018 High-quality sequential-vapor-deposited Cs 2 AgBiBr 6 thin films for lead-free perovskite solar cells (Solar RRL 12/2018) *Sol. RRL* **2** 1870238
[50] Eggers H *et al* 2020 Inkjet-printed micrometer-thick perovskite solar cells with large columnar grains *Adv. Energy Mater.* **10**
[51] Xingtian Y, Meidan Que Y X and Que W 2015 High efficiency hysteresis-less inverted planar heterojunction perovskite solar cells with a solution-derived NiOx hole contact layer *J. Mater. Chem. A Mater.* **3** 24495–503
[52] Ihteaz M *et al* 2019 Scalable processing of low-temperature TiO2 nanoparticles for high-efficiency perovskite solar cells *American Chemical Society* **2** 47–58
[53] Arjun Singh S K G and Garg A 2017 Inkjet printing of NiO films and integration as hole transporting layers in polymer solar cells *Sci. Rep.* **1775** 1–12
[54] Strobel N, Seiberlich M, Eckstein R, Lemmer U and Hernandez-Sosa G 2019 Organic photodiodes: Printing, coating, benchmarks, and applications *Flex. Print. Electron.* **4** 1–28
[55] Shan S *et al* 2021 Manipulating the film morphology evolution toward green solvent-processed perovskite solar cells *SusMat.* **1** 537–44
[56] Kwon N, Lee J, Ko M J, Kim Y Y and Seo J 2023 Recent progress of eco-friendly manufacturing process of efficient perovskite solar cells *Nano Converg* **10**
[57] Gao W *et al* 2018 High-quality Cs2AgBiBr6 double perovskite film for lead-free inverted planar heterojunction solar cells with 2.2 % efficiency *Chem Phys Chem* **19** 1696–700
[58] Barrows A T, Pearson A J, Kwak C K, Dunbar A D F, Buckley A R and Lidzey D G 2014 Efficient planar heterojunction mixed-halide perovskite solar cells deposited via spray-deposition *Energy Environ. Sci.* **7** 2944–50
[59] Chang W C, Lan D H, Lee K M, Wang X F and Liu C L 2017 Controlled deposition and performance optimization of perovskite solar cells using ultrasonic spray-coating of photoactive layers *ChemSusChem* **10** 1405–12
[60] Bishop J E *et al* 2018 High-efficiency spray-coated perovskite solar cells utilizing vacuum-assisted solution processing *ACS Appl. Mater. Interfaces* **10** 39428–34
[61] Kim J *et al* 2017 Overcoming the challenges of large-area high-efficiency perovskite solar cells *ACS Energy Lett.* **2** 1978–84
[62] Heo J H *et al* 2021 Efficient and stable graded CsPbI3−xBrx perovskite solar cells and submodules by orthogonal processable spray coating *Joule* **5** 481–94
[63] Huang H, Shi J, Zhu L, Li D, Luo Y and Meng Q 2016 Two-step ultrasonic spray deposition of CH3NH3PbI3 for efficient and large-area perovskite solar cell *Nano Energy* **27** 352–8
[64] Ning W *et al* 2018 Long electron-hole diffusion length in high- quality lead-free double perovskite films **30**
[65] Lan D H, Hong S H, Chou L H, Wang X F and Liu C L 2018 High throughput two-step ultrasonic spray deposited CH3NH3PbI3 thin film layer for solar cell application *J. Power Sources* **390** 270–7
[66] Shadabroo M S, Abdizadeh H and Golobostanfard M 2021 Dimethyl Sulfoxide Vapor-Assisted Cs2 AgBiBr6 Homogenous Film Deposition for Solar Cell Application *ACS Appl. Energy Mater.* **4** 6797–805
[67] Luo T *et al* 2020 Dual interfacial engineering for efficient Cs2AgBiBr6 based solar cells *Journal of Energy Chemistry* **53** 372–8
[68] Yang X *et al* 2020 Simultaneous power conversion efficiency and stability enhancement of Cs2AgBiBr6 lead-free inorganic perovskite solar cell through adopting a multifunctional dye interlayer *Adv. Funct. Mater.* **30** 1–8
[69] Wu C *et al* 2018 Highly efficient and stable self-powered ultraviolet and deep-blue photodetector based on Cs2AgBiBr6/SnO2 heterojunction *Adv. Opt. Mater.* **6** 1–7
[70] Li J *et al* 2020 Alkali metal ion-regulated lead-free, all-inorganic double perovskites for HTM-free, carbon-based solar cells *ACS Appl. Mater. Interfaces* **12** 47408–15
[71] Pantaler M *et al* 2018 Hysteresis-free lead-free double-perovskite solar cells by interface engineering *ACS Energy Lett.* **3** 1781–6
[72] Wang B *et al* 2021 Chlorophyll derivative-sensitized TiO 2 electron transport layer for record E ffi ciency of Cs 2 AgBiBr 6 double perovskite solar cells *J. Am. Chem. Soc.* **143** 2207–11
[73] Zhao X G, Yang D, Ren J C, Sun Y, Xiao Z and Zhang L 2018 Rational design of halide double perovskites for optoelectronic applications *Joule* **2** 1662–73
[74] Wang M *et al* 2018 High-quality sequential-vapor-deposited Cs2AgBiBr6 thin films for lead-free perovskite solar cells *Sol. RRL* **2** 1–6
[75] López M L, Veiga M L and Pico C 1994 Cation ordering in distorted perovskites (MLa) (MgTe)O6, M = Na, K *J. Mater. Chem.* **4** 547–50
[76] Li Z *et al* 2021 Understanding the role of grain boundaries on charge-carrier and ion transport in Cs2AgBiBr6 thin films *Adv. Funct. Mater.* **31**
[77] Liu S, Zhang H, Xing Y, He Q, Han S and Zhu H 2023 Thermodynamically regulated preparation of high performance for carbon-based Cs2AgBiBr6 perovskite solar cells *Mater. Sci. Semicond. Process.* **154** 107193
[78] Schmitz F *et al* 2022 High open-circuit voltage Cs2AgBiBr6 carbon-based perovskite solar cells via green processing of ultrasonic spray-coated carbon electrodes from waste tire sources *ChemSusChem* **15**

[79] Zhao D et al 2022 Overcoming the limitation of Cs2AgBiBr6 double perovskite solar cells through using mesoporous TiO2 electron extraction layer *Energy and Environmental Materials* **5** 1317–22
[80] Li B et al 2022 Efficient and stable Cs2AgBiBr6 double perovskite solar cells through in-situ surface modulation *Chem. Eng. J.* **446** 137144
[81] Ou Y et al 2022 Efficiency improvement of Cs2AgBiBr6 perovskite solar cells with modification of SnS quantum dots *Mater. Lett.* **312**
[82] Yang A, Zhang L, Xu Y, Wang Q, Lyu M, Lu H and Zhu J 2022 VOC over 1.2 V for Cs2AgBiBr6 solar cells based on formamidinium acetate additive *J. Mater. Sci., Mater. Electron.* **33** 18758–67
[83] Sirtl M T et al 2022 2D/3D hybrid Cs2AgBiBr6 double perovskite solar cells: improved energy level alignment for higher contact-selectivity and large open circuit voltage *Adv. Energy Mater.* **12**
[84] Pang B et al 2022 Improved charge extraction and atmospheric stability of all-inorganic Cs2AgBiBr6 perovskite solar cells by MoS2 nanoflakes *Sol. Energy Mater. Sol. Cells* **246** 111932
[85] Li J et al 2022 Pinning bromide ion with ionic liquid in lead-free Cs2AgBiBr6 double perovskite solar cells *Adv. Funct. Mater.* **32** 2112991
[86] Ou Y et al 2022 Boosting the stability and efficiency of Cs2AgBiBr6 perovskite solar cells via Zn doping *Opt Mater (Amst)* **129** 112452
[87] Fu Q et al 2018 Recent progress on the long-term stability of perovskite solar cells *Adv. Sci.* **5**
[88] Spencer M G and Alam T 2019 High power direct energy conversion by nuclear batteries *Appl. Phys. Rev.* **6**
[89] Xiao Z, Meng W, Wang J and Yan Y 2016 Thermodynamic stability and defect chemistry of bismuth-based lead-free double perovskites *Chem Sus Chem* **9** 2628–33
[90] Xu X, Zhong Y and Shao Z 2019 Double perovskites in catalysis, electrocatalysis, and Photo(electro)catalysis *Trends Chem.* **1** 410–24
[91] Li Z et al 2021 Single-layered mxene nanosheets doping TiO_2 for efficient and stable double perovskite solar cells *J. Am. Chem. Soc.* **143** 2593–600
[92] Ghasemi M et al 2020 Dual-ion-diffusion induced degradation in lead-free Cs2AgBiBr6 double perovskite solar cells *Adv. Funct. Mater.* **30** 2002342
[93] Wang T, Yue D, Li X and Zhao Y 2020 Lead-free double perovskite Cs2AgBiBr6/RGO composite for efficient visible light photocatalytic H_2 evolution *Appl. Catal.* B **268** 118399
[94] Wang Y et al 2021 Lead-free perovskite Cs2AgBiBr6@g-C3N4 Z-scheme system for improving CH_4 production in photocatalytic CO_2 reduction *Appl Catal* B **282**
[95] Zhou J, Xia Z, Molokeev M S, Zhang X, Peng D and Liu Q 2017 Composition design, optical gap and stability investigations of lead-free halide double perovskite Cs2AgInCl6 *J. Mater. Chem. A Mater.* **5** 15031–7
[96] Zhou J, Rong X, Molokeev M S, Zhang X and Xia Z 2018 Exploring the transposition effects on the electronic and optical properties of Cs2AgSbCl6: Via a combined computational-experimental approach *J. Mater. Chem. A Mater.* **6** 2346–52
[97] Dong L et al 2018 Elastic properties and thermal expansion of lead-free halide double Cs2AgBiBr6 *Comput. Mater. Sci.* **141** 49–58
[98] Zhang Z et al 2019 Stable and highly efficient photocatalysis with lead-free double-perovskite of Cs2AgBiBr6 *Angewandte Chemie - International Edition* **58** 7263–7
[99] Dong L et al 2018 Elastic properties and thermal expansion of lead-free halide double perovskite Cs2AgBiBr6 *Comput. Mater. Sci.* **141** 49–58
[100] Faghihnasiri M, Beheshtian J, Shayeganfar F and Shahsavari R 2020 Phase transition and mechanical properties of cesium bismuth silver halide double perovskites (Cs2AgBiX6, X = Cl, Br, I): A DFT approach *Phys. Chem. Chem. Phys.* **22** 5959–68
[101] Ghebouli M A, Chihi T, Ghebouli B and Fatmi M 2018 Study of the structural, elastic, electronic and optical properties of lead free halide double perovskites Cs2AgBiX6(X = Br, Cl) *Chin. J. Phys.* **56** 323–30
[102] Su J, Mou T, Wen J and Wang B 2020 First-principles study on the structure, electronic, and optical properties of Cs 2 AgBiBr 6 - *Physical Chemistry* **124** 5371–7
[103] Nabi M and Gupta D C 2021 Potential lead-free small band gap halide double perovskites Cs2CuMCl6 (M = Sb, Bi) for green technology *Sci. Rep.* **11** 1–13
[104] Kibbou M, Haman Z, Essaoudi I and Ainane A 2023 Designing new halide double perovskite materials Rb2AgGaX6 (X: Br, Cl) with direct band gaps and high power conversion efficiency *J. Solid State Chem.* **317**
[105] Guechi N, Bouhemadou A, Bin-Omran S, Bourzami A and Louail L 2018 Elastic, optoelectronic and thermoelectric properties of the lead-free halide semiconductors Cs2AgBiX 6 (X = Cl, Br): Ab Initio Investigation *J. Electron. Mater.* **47** 1533–45
[106] Li Z, Xu Q, Sun Q, Hou Z and Yin W J 2019 Thermodynamic stability landscape of halide double perovskites via high-throughput computing and machine learning *Adv. Funct. Mater.* **29** 1–9
[107] Bealing C R, Baumgardner W J, Choi J J, Hanrath T and Hennig R G 2012 Predicting nanocrystal shape through consideration of surface-ligand interactions *ACS Nano* **6** 2118–27
[108] Filip M R, Liu X, Miglio A, Hautier G and Giustino F 2018 Phase diagrams and stability of lead-free halide double perovskites Cs2BB′ X6: B = Sb and Bi, B′ = Cu, Ag, and Au, and X = Cl, Br, and i *J. Phys. Chem.* C **122** 158–70
[109] Liao H G et al 2014 Facet development during platinum nanocube growth *Science* **345** 916–9
[110] Puttisong Y et al 2020 Effect of crystal symmetry on the spin states of fe and vibration modes in lead-free double perovskite Cs AgBi (Fe) Br effect of crystal symmetry on the spin states of Fe 3 + and vibration modes *J Phys Chem Lett.* **11** 4873–8
[111] Xiao B, Tan Y, Yi Z, Luo Y, Jiang Q and Yang J 2021 Band matching strategy for all-inorganic Cs 2 AgBiBr 6 double perovskite solar cells with high photovoltage *ACS Appl. Mater. Interfaces* **13** 37027–34
[112] Bi E et al 2017 Diffusion engineering of ions and charge carriers for stable efficient perovskite solar cells *Nat. Commun.* **8** 15330
[113] Li N et al 2019 Cation and anion immobilization through chemical bonding enhancement with fluorides for stable halide perovskite solar cells *Nat. Energy* **4** 408–15
[114] William Shockley H J Q 1961 Detailed balance limit of efficiency of p-n junction solar cells *J. Appl. Phys.* **32** 510–9
[115] Rahane S N et al 2024 Lead-Free Cs2AgBiCl6 double perovskite: experimental and theoretical insights into the self-trapping for optoelectronic applications *ACS Physical Chemistry Au* **4** 476–89
[116] Locardi F et al 2018 Colloidal synthesis of double perovskite Cs2AgInCl6 and Mn-doped Cs2AgInCl6 nanocrystals *J. Am. Chem. Soc.* **140** 12989–95
[117] Tran T T, Panella J R, Chamorro J R, Morey J R and McQueen T M 2017 Designing indirect-direct bandgap transitions in double perovskites *Mater Horiz* **4** 688–93
[118] Du K Z, Meng W, Wang X, Yan Y and Mitzi D B 2017 Bandgap engineering of lead-free double perovskite Cs2AgBiBr6 through trivalent metal alloying *Angewandte Chemie - International Edition* **56** 8158–62
[119] Hutter E M, Ge C, Bartesaghi D, Grozema F C and Savenije T J 2018 Band-like charge transport in Cs 2 AgBiBr 6 and mixed antimony − bismuth Cs 2 AgBi 1 − x Sb x Br 6 halide double perovskites *ACS Omega* **3** 11655–62

[120] Meng W, Wang X, Xiao Z, Wang J, Mitzi D B and Yan Y 2017 Parity-forbidden transitions and their impact on the optical absorption properties of lead-free metal halide perovskites and double perovskites *J. Phys. Chem. Lett.* **8** 2999–3007
[121] Pan W *et al* 2017 Cs2AgBiBr6 single-crystal x-ray detectors with a low detection limit *Nat. Photonics* **11** 726–32
[122] Li Q *et al* 2017 High-pressure band-gap engineering in lead-free Cs2AgBiBr6 double perovskite *Angewandte Chemie - International Edition* **56** 15969–73
[123] Kumar Chini M, Goverapet Srinivasan S, Tailor N K, Yukta, Salahub D and Satapathi S 2020 Lead-free, stable mixed halide double perovskites Cs2AgBiBr6 and Cs2AgBiBr6−xClx—A detailed theoretical and experimental study *Chem. Phys.* **529**